

Draft Final Report

**EVALUTATION OF THE JULY 31, 2000 OZONE EPISODE
IN THE SAN FRANCISCO BAY AREA
WITH THE PROCESS ANALYSIS TOOL**

Prepared for

The Bay Area Air Quality Management District
Modeling Advisory Committee
San Francisco, CA

Prepared by

William Vizuete
Dr. David T. Allen
University of Texas at Austin
Center for Energy and Environmental Resources

Chris Emery
Greg Yarwood
ENVIRON International Corporation

Dr. Harvey Jeffries
University of North Carolina at Chapel Hill

March 15, 2004



TABLE OF CONTENTS

	Page
INTRODUCTION.....	1
Conceptual Model Of Process Analysis	1
Process Analysis Output	3
EVALUATION OF SAN FRANCISCO BAY AREA	7
Methodology	7
Results	8
Northern Analysis Region.....	8
Southern Analysis Region.....	10
Conclusions.....	11
REFERENCES.....	13

FIGURES

Figure 1. Conceptual model explaining processes that contribute to changes in pollutant concentrations	14
Figure 2. Models are formulated using “well-mixed” chemical reactor cells that hold concentration information and are subject to a collection of processes that modify those concentrations over short time steps	14
Figure 3. Conceptual drawing of the CAMx grid cell network of many “well-mixed cells” coupled together via cell to cell transport can either be by advection or by diffusion.....	15
Figure 4. Example Process Analysis time series plot with observed hourly averaged observations	16
Figure 5. Conceptual model of the radical and nitrogen oxides chemical cycles resulting in ozone production.....	17
Figure 6. example of the Process Analysis Radical and Nitrogen Cycles diagram	18
Figure 7. (A) The location of the 640 km ² sub-domain, outlined in black, used by the process analysis tool for the northern source region. (B) A close up view of the sub-domain. The black dots represent the lower left corner of the 4 km CAMx grid cells. Observed data was used from the monitor stations that are highlighted on the map.....	19



March 15, 2004

Figure 8. A) The location of the 640 km² sub-domain, outlined in black, used by the process analysis tool for the southern ozone region. (B) A close up view of the sub-domain. The black dots represent the lower left corner of the 4 km CAMx grid cells. Observed data was used from the monitor stations that are highlighted on the map.....20

Figure 9. Graph of the Kv parameter versus CAMx model heights for hour 19. Each line on the graph represents a grid cell within the process analysis sub-domain for the northern source region. These values were used to determine the mixing height at each hour within the domain. At this hour the mixing height was determined to extend through layer 5.21

Figure 10. The evolution of the mixing height within the process analysis sub-domain for the (A) northern and (B) southern region. The x-axis represents the hours of the simulation day and the modeling height is shown vertically. The black horizontal grid lines represent the CAMx grid layers and the red line is the mixing height. The light blue and yellow boxes show the layers that were entrained and detrained, respectively.22

Figure 11. Graph of horizontal and vertical flows within the process analysis box for the northern source region. The fraction of the box advected per hour is represented on the y-axis and hours within the simulation day on the x-axis. In the morning hours there is a net horizontal flow into the box resulting in pollutants being advected out vertically. In the late morning this phenomena is reversed and pollutants are being advected vertically into the box through the afternoon and night hours.23

Figure 12. Volatile organic carbon (VOC) to NOx ratios for the process24

Figure 13. Nitrogen compound percent composition of the process analysis box based on cell concentration as a function of time for the northern source region.24

Figure 14. (A) NO₂ and (B) O₃ model concentrations and the processes that contribute to the final concentration for the northern source region25

Figure 15. (A) Volatile organic compound percent composition of the process analysis box based on cell emissions and (B) cell concentration as a function of time for the northern source region.26

Figure 16. Olefin model concentrations and the processes that contribute to the final concentration for the northern source region. Observed data is shown from the Bethel Island (BTI) monitor station as a three hour average.....27

Figure 17. ALD2, a class of aldehydes, model concentrations and the processes that contribute to the final concentration for the northern source region. Observed data is shown from the Bethel Island (BTI) monitor station as a three hour average.....27

Figure 18. Ozone production diagram including radical and NOx cycles in the northern source region for hours 8-18.....28

Figure 19. Distribution of the final NOy in the northern source region for hours 8-18.....28



March 15, 2004

Figure 20. Ozone model concentrations and the processes that contribute to the final concentration for the northern ozone region. Observed data are shown from three monitor stations (BTI, KRE, PBG) as one hour averages.29

Figure 21. Graph of horizontal and vertical flows within the process analysis box for the southern ozone region. The fraction of the box advected per hour is represented on the y-axis and hours within the simulation day on the x-axis. In the morning hours there is a net horizontal flow out the box resulting in pollutants being advected in vertically. This phenomenon continues throughout the day except for a few hours in the late evening.....30

Figure 22. Nitrogen compound percent composition of the process analysis box based on cell concentration as a function of time for the southern ozone region.....31

Figure 23. Volatile organic carbon (VOC) to NOx ratios for the process analysis box in ppb C for the southern ozone region.....31

Figure 24. (A) Volatile organic compound percent composition of the process analysis box based on cell emissions, and (B) cell concentration as a function of time for the southern ozone region.....32

Figure 25. Olefin model concentrations and the processes that contribute to the final concentration for the southern ozone region. Observed data is shown from the Sunol (SUNO) monitor station as a one hour average.33

Figure 26. Toluene model concentrations and the processes that contribute to the final concentration for the southern ozone region. Observed data is shown from the Sunol (SUNO) monitor station as a one hour average.33

Figure 27. Xylene model concentrations and the processes that contribute to the final concentration for the southern ozone region. Observed data is shown from the Sunol (SUNO) monitor station as a one hour average.....34

Figure 28. ALD2, a classification of aldehydes, model concentrations and the processes that contribute to the final concentration for the southern ozone region. Observed data is shown from the Sunol monitor station as a one hour average.34

Figure 29. Ozone production diagram including radical and NOx cycles in the southern ozone region for hours 8-18.35

Figure 30. Ozone yield per VOC for hours 8-18 for (A) the northern source region and (B) southern ozone region.....36

Figure 31. Distribution of the final NOy in the southern ozone region for hours 8-1837

Figure 32. Ozone model concentrations and the processes that contribute to the final concentration for the southern ozone region. Observed data is shown from two Livermore monitor stations (LVF,LVR1) as one hour averages.38



March 15, 2004

INTRODUCTION

It is generally known that ozone differs from other major air pollutants in several important ways (Seinfeld and Pandis, 1998). Ozone formation is dependent on reactions involving two principal classes of pollutants, NO_x and VOC. The formation of O₃ is complex and nonlinear, involving hundreds of chemical reactions. Because some of the reactions are photolytic, concentrations are critically dependent upon meteorology. As a result, ozone formation varies geographically, diurnally, and seasonally. There is also wide recognition that ozone and its precursors can be transported over local, regional and global scales. Developing control strategies for atmospheric pollutants requires the development of comprehensive mathematical models that can describe the interplay of multiple complex systems. Current gridded photochemical air quality models, commonly used in the development and evaluation of air quality regulations, calculate the rates of atmospheric processes that control air pollutant concentrations. These processes include chemical formation, chemical consumption, advection, diffusion, and deposition. In the photochemical model, these processes are coupled into a system of mass continuity equations used to predict the species concentrations in each grid cell (Russell and Dennis, 2000). Many models output only the spatial and temporal distribution of species concentrations. Descriptions of the individual processes that lead to these changes in species concentrations are not recorded. With only concentration fields, it is difficult to infer why air pollutant concentrations change or to understand the relationship among grid cells. A detailed evaluation of these individual processes will lead to an increased understanding of the formation processes for pollutants.

“Process analysis” refers to techniques to quantitatively track individual physical and chemical process that contribute to changing pollutant concentrations for a grid cell or collection of grid cells within photochemical grid models. Process analysis provides dynamic information such as horizontal and vertical pollutant fluxes crossing cell boundaries, chemical production and consumption rates, emission rates, deposition rates, and initial and final concentrations. Much of the original development of the Process Analysis Tool (PAT) to be described in this report was undertaken at the University of North Carolina (UNC) at Chapel Hill (Tonnesen, 1995). This was officially incorporated into Version 3 of the Comprehensive Air quality Model with extensions (CAMx) and has been carried forward in the latest versions of the photochemical model (ENVIRON, 2004). The PAT has since been further modified by the University of Texas (UT) at Austin and UNC for analysis of ozone in southeast Texas (Vizueté *et al.*, 2004). The latest PAT was designed to gain a better understanding of atmospheric reaction networks and to improve our ability to characterize the chemistry that leads to poor air quality. The following is a general discussion on the concepts that form the foundation of the process analysis tool.

Conceptual Model of Process Analysis

Figure 1 is an illustration of the conceptual basis of a “process-based” photochemical grid model. Concentrations of pollutants at every time step are determined by a set of processes that describe the physical and chemical changes that are occurring. Various physical and chemical processes that affect the species concentrations are represented in the model by various fluxes of mass, momentum, and energy. These processes are described by sets of differential equations that calculate the changes in species concentrations. When these processes are allowed to operate simultaneously for a small amount of time, changes in species concentrations over a time step are

March 15, 2004

predicted. This “marching in time” technique can be used to advance a given initial concentration to a future time by repeating many incremental steps. Therefore, it is possible to step from a known present state to a future state by many different pathways and combinations of processes. For example, different dilution volumes when combined with different emission intensities can result in predicting identical future concentrations. A low emissions rate of a species can be compensated for by a low mixing volume and vice versa.

This conceptual model is implemented in a photochemical grid model as “well-mixed” environmental volumes, or grid cells as shown in Figure 2. These grid cells are subjected to a mass balance at each time step. The resolution of these grid cells can vary vertically and horizontally and is dependent on computing costs. The air quality model utilized in this analysis applied a 4 by 4 km horizontal resolution for its grid cells. In the model these grid cells can extend vertically from 20 to 1000 meters. Figure 3 shows that many well-mixed grid cells are coupled together via cell-to-cell transport through all faces in common with other adjacent cells. This cell-to-cell transport can either be by advection or by diffusion. In air quality models, the rates of all these processes for each cell are added together and the combined effect is integrated and added to the initial state to predict the subsequent state. Only the resulting species concentrations are saved and all information concerning how these concentrations were achieved is normally lost.

As stated previously, atmospheric ozone chemistry is a highly non-linear feedback-controlled system, with buffers and auto-catalytic behavior (Seinfeld and Pandis, 1998). Both physical and chemical processes compete to change predicted species concentrations. This complex system makes it virtually impossible to understand how the model arrived at certain predictions. This causes difficulties in answering common problems such as why predicted species concentrations differ from real-world observations. Without the insights provided by the process analysis tool the reasons for model failures are not self-evident. By focusing attention on the individual processes and their interactions in achieving the model’s predictions, process analysis can provide significant understanding of which parts of the modeling system are producing results. The information that is gained can result in identifying whether certain model inputs or processes need improvement or warrant further investigation. The following is a detailed description of the type of output that is generated by the process analysis tool.

In CAMx, additional code was added to integrate each of these processes separately and the information is saved to the integrated process rate (IPR) and the integrated reaction rate (IRR) output files. With these extra data the model’s performance can be further analyzed and visualized with the PAT to reveal the model’s calculations. Post processing algorithms for analyzing these files were originally created at UNC (Tonnesen, 1995). Recent modifications by UT and UNC were made to adapt these tools to analyze model performance in Southeast Texas (Vizuete *et al.*, 2004). Because information concerning chemical transformations is paramount for a detailed analysis of modeling phenomena, additional code was added to CAMx by Vizuete *et al.* to ensure that the explicit descriptions of these transformations were saved. The code integrates the rate of each chemical reaction at the same time that the rates of change of the species concentrations are being integrated. The PAT now presents as Excel spread sheets the various chemical processes such as initiation, propagation, and termination and cyclic reactions caused by changes in the species concentrations during the time step.



March 15, 2004

Process Analysis Output

The PAT produces a significant amount of information that ultimately leads to the creation of two spreadsheets entitled “time series” and “cycles”. These spreadsheets display up to 40 graphs for a single day’s simulation. In the time series spreadsheet several graphs are used to show the physical conditions of the focus region under analysis. In addition to this information, the magnitudes of the various processes over the course of the day are shown for all active species. A series of graphs that show the various processes verses time are used to detail this data. Finally, the initialization, propagation, and termination processes in the chemistry are illustrated and distributions of competitive pathways in the chemistry are shown in the cycle spreadsheet.

Figure 4 shows an example of a time series plot that illustrates the process rates and model concentrations versus time (Tesche *et al.*, 2004; Vizuete *et al.*, 2004). This graph closely follows the concepts shown in Figure 2, where the model concentration is given for each hour and the magnitudes of the various processes are shown as different colored lines. In these graphs the chemistry change is the net change due to multiple reaction pathways, but time series plots alone are not capable of explaining the contributions of specific reaction pathways to the net change. A different type of analysis detailed in the cycle spreadsheet is required to achieve this. The theory and a detailed explanation of the diagrams used in the cycle spreadsheet is described next.

Ozone (O_3) is not emitted directly from sources, but is formed by chemical reactions in the atmosphere (Seinfeld and Pandis, 1998). Combustion processes emit mostly NO which is rapidly oxidized to NO_2 in the ambient air. In sunlight, the NO_2 is photolyzed to produce NO and atomic oxygen, $O(^3P)$. The atomic oxygen then reacts with molecular oxygen to form O_3 . Therefore, the photolysis of NO_2 is the major source of O_3 in the troposphere. This ozone can immediately react with NO to produce NO_2 again. In the absence of competing reactions, NO, NO_2 , and O_3 reach equilibrium and the amount of O_3 never exceeds the amount of NO_x ($NO+NO_2$).

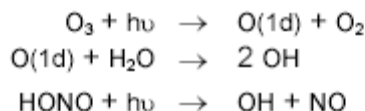
However, if volatile organic compounds (VOCs) are present in the system then free radicals, generated from the oxidative degradation of VOCs, oxidize NO to NO_2 . This oxidation results in accumulation of the O_3 formed in the NO_2 photolysis and thereby causes a net increase in O_3 . Since the NO can be reused several times in these conditions, the amount of O_3 can now be many times the amount of NO_x . The free radicals are products of the reactions involving hydroxyl radicals, OH, with VOC and CO. The major pathways that produce OH radicals are the photolysis of ozone and aldehydes. The HO_2 and RO_2 radicals compete with O_3 for NO. Each time a radical oxidizes an NO, an O_3 accumulates and another NO_2 is generated. This NO_2 can again photolyze to create yet another O_3 . Eventually the reaction of NO_2 with several of the radicals forms nitrogen products such as nitric acid (HNO_3) and organic nitrates, terminating the production of O_3 from that particular NO molecule. In the Carbon Bond IV mechanism used by the model in this study, new OH radicals are produced directly and indirectly by the following reactions:



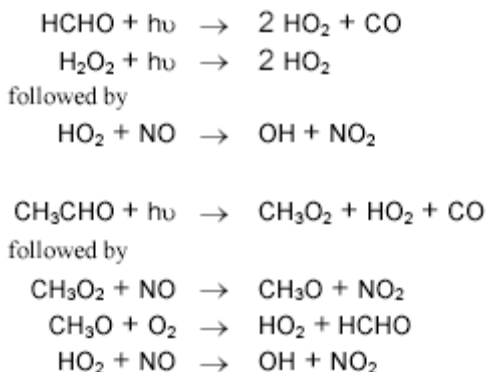
March 15, 2004

Radical Initiation Reactions

Direct OH:

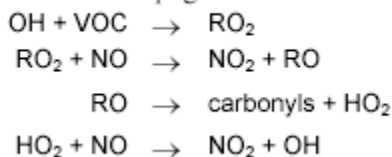


Indirect OH:



Following radical initiation, VOCs are oxidized and NO-to-NO₂ conversion occurs in radical propagation steps. The following reaction steps illustrate a propagation chain where a VOC molecule is converted to one or more carbonyl molecules and two molecules of NO are converted to two molecules of NO₂. Note that the free radical emerges as OH again at the end of the chain. In these chains, the initial OH could be either a new OH or a re-created OH:

Radical Propagation Reactions



The radical propagation stops when the reacting radicals are incorporated into stable products. The following are the radical termination steps:

Radical Termination Reactions

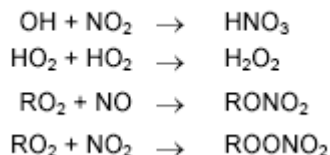


Figure 5 shows a schematic in which the OH initiation, propagation, and termination and the NO emissions, oxidation, and photolysis cycles are combined. Here the NO_x and radical cycles that show the re-creation of OH and of NO are made explicit. The named quantities in the figure are repeated here:



March 15, 2004

- q = "new OH" radicals produced by photolysis, ppb
 Q = "total OH" radicals reacting, ppb: $Q = q + q P_r + q P_r^2 + \dots = q / (1 - P_r)$
 P_r = OH propagation factor, <1.0 due to termination
 e = "new NO" from emissions, ppb
 E = "total NO" reacting, ppb: $E = e + e P_n + e P_n^2 + \dots = e / (1 - P_n)$
 P_n = NO propagation factor, <1.0 due to termination
 f = net O₃ yield from NO₂ photolysis

The term P_r represents the fraction of OH that propagates via reactions with VOC, and $1 - P_r$ is essentially the fraction of OH that reacts with NO₂ to make HNO₃. Similarly, the term P_n represents the fraction of NO₂ that is photolyzed, and $1 - P_n$ symbolizes the fraction of NO₂ that is converted to termination products (HNO₃, RNO₃) or is lost by physical processes like deposition and horizontal or vertical transport.

An example of an application of a cycle diagram is shown in Figure 6, which is for a UAM application in Charlotte, NC over a 6 x 6, 5-km aggregated cell area covering the downtown region (Jeffries *et al.*, 1997). The numerical values in this figure are typical of conditions that led to ozone near the one-hour standard. Charlotte is in general NO_x limited, but the core city are near the optimum ozone production conditions. This is evident in that the NO_x is nearly completely consumed by the end of the daylight period.

For NO_x limited conditions, new O₃ is explained by the following:

$$\text{new O}_3 = E * P_n * f$$

where

- E = (new NO) $[1 / (1 - P_n)]$ = total NO oxidized to NO₂
 P_n = fraction of all NO₂ that is photolyzed
 f = fraction of all NO₂ photolysis reactions that make ozone

Using the values in Figure 6, new NO = 49.0 ppb, $P_n = 0.731$, $f = 0.937$. Therefore (new O₃)/(new NO) = 2.54.

For radical limited conditions, new O₃ is explained by the following:

$$\text{new O}_3 = (\text{VOC reacted}) * R * P_n * f$$

where

- (VOC reacted) = (new OH) $[1 / (1 - P_r)]$ + (VOC photolyzed)
 R = (NO → NO₂) / (VOC reacted) essentially a type of "mixture reactivity"
 P_n = fraction of all NO₂ that photolyzes
 f = fraction of all NO₂ photolysis reactions that make ozone

Using the values in Figure 6, new OH = 27.9 ppb, $P_r = 0.757$, $R = 1.26$, (new O₃)/(new OH) = 4.46.



March 15, 2004

These two values are the “gain” or “chemical amplification” of the system. If there is sufficient NO_x, then for 1 ppb of new OH radical created, there will be 4.4 ppb ozone created. From the NO_x viewpoint, if there are sufficient sources of peroxy radicals, then for every 1 ppb of NO emitted, there will be 2.5 ppb ozone created. In conclusion, there are a set of chemical process parameters that determine how much new O₃ can be produced in a system. Proper analysis of the chemical production of ozone must take into account these parameters:

- Availability of NO
- Ability of the system to create new OH radicals, which depends on the VOC composition
- Radical propagation factor (which depends on the ratio of VOC/NO_x)
- General reactivity of the VOC mixture, which depends on the VOC composition
- Relative competition between the physical removal processes for NO₂ and its photolysis rate

Several of these factors depend upon the availability of NO_x and VOC, which is consistent with the well known relationship between ozone formation and VOC/NO_x ratio. Moreover, the cycle analysis in PA reveals the underlying effects of VOC/NO_x ratio leading to a deeper understanding of ozone formation.



March 15, 2004

EVALUATION OF THE SAN FRANCISCO BAY AREA

The following sections will detail the methodology, results, and conclusions when a photochemical grid model in conjunction with the PAT was used to study modeling phenomena in the San Francisco Bay Area during the Central California Ozone Study (CCOS) episode of July 30 – August 2, 2000. This project employed CAMx v4.03, a publicly available computer modeling system for the integrated assessment of photochemical and particulate air pollution. The process analysis code modifications, as described above, were applied to CAMx by UT. ENVIRON configured that version of the model to run a process analysis domain over the San Francisco Bay Area and ran the model for the July 30 – August 2, 2000 episode. Evaluation of the IPR and IRR output generated for the Bay Area PA domain was then performed by UT. The focus of the analysis was on the key episode day of interest, July 31, 2000. The following section details the methodology used to accomplish this work.

Methodology

The first step in the process analysis procedure is to generate the necessary files from the photochemical grid model. A procedure to enable process analysis output in CAMx is outlined in detail within the CAMx User Guide, Chapter 7 "PROCESS ANALYSIS" (ENVIRON, 2004). The "Technology type" flag was set to "PA" to generate both *.irr and *.ipr output files. UT provided additional code to the official release to allow CAMx to output data concerning air fluxes into the IPR file. These two files represent the only data needed from the photochemical grid model to input into the PAT. The PAT generated two final Microsoft Excel files, *.timeseries.xls and *.cycles.xls. The following will outline the process involved in utilizing the PAT to obtain the desired output files.

The process analysis tool aggregates CAMx grid cells horizontally and model layers vertically resulting in a single large cell that effectively mimics a box model. This large cell, or process analysis box (PAB), represents the total system that the PAT analyzes. Pollutant fluxes are calculated crossing the boundary of this box and source and sink rates are represented within the box. The selection of the PAB is an iterative process and represents the most challenging part of the methodology. The goal is to define a PAB that captures the modeling phenomena under investigation without diluting the characteristics of the performance in question with a large box. In contrast, a box of inadequate dimension will result in the dominance of transport processes erasing the chemical features of the modeling event. The location of the box is also a consideration. Large emission sources relatively close to the boundaries of the PAB may have to be incorporated. Sizeable concentration gradients will cause transport processes to dominate over all other rates. Vertically, the height of the sub-domain should match the evolution of the planetary boundary layer or mixing height throughout the simulation day.

For this analysis two areas in the eastern San Francisco Bay Area were chosen. A northern domain was chosen to evaluate the region where the model predicts high ozone concentrations in the east bay. The southern domain was chosen to evaluate the region where the model under predicts the highest ozone recorded in the Bay Area. The horizontal domain chosen for the northern source region is represented in Figure 7. The 640 km² sub-domain encompasses a heavily industrial and suburban area along the Sacramento River. The southern region of this



March 15, 2004

sub-domain consists largely of natural terrain, including Mt. Diablo State Park with a mountain peak 1,170 meters above sea level. This domain was chosen to include the source region near the river in addition to the region of high modeled ozone concentrations over the park area. This domain also contains three ground monitor stations where observed concentrations of NO, NO₂, ozone, and certain volatile organic carbons (VOC) were recorded. The location of these stations and the data collected at the stations are shown on the map.

The horizontal domain chosen for the southern ozone region is represented in Figure 8. The 640 km² sub-domain includes several interstate highways with heavy traffic activity and suburban areas. The northern and eastern region of this sub-domain consists largely of natural, hilly terrain. This domain contains four ground monitor stations where observed concentrations of NO, NO₂, ozone, and certain volatile organic carbons (VOC) were recorded. The location of these stations and the data collected at the station are shown on the map.

The next step is to determine the mixing height within these domains. The PAT allows the process analysis box to follow changes in mixing height throughout the simulation day. In the CAMx model vertical mixing is a function of the layer interface diffusivity or “Kv” value. These values can vary spatially and temporally due to the heterogeneity of terrain and meteorological conditions. An incorrect input of mixing heights into the PAT will result in large vertical transport of pollutants across the top boundary. This is an undesired result as it will mask the important chemical processes that are occurring throughout the planetary boundary layer (i.e., ventilating the box model).

Mixing heights were determined by qualitatively analyzing the evolution of the Kv values for each grid cell in the PAB. Figure 9 shows an example of a graph of Kv parameter values versus CAMx model heights for hour 19 in the northern domain; each line on the graph represents a grid cell within the PAB. These values were used to determine the mixing height at each hour within the domain. At this hour the mixing height was determined to extend up through layer 5. Figure 10 shows the evolution of the mixing height within the process analysis box for the northern and southern PABs. The x-axis represents the hours of the simulation day and the modeling height is shown vertically. The black horizontal grid lines represent the CAMx grid layers and the red line is the mixing height. The light blue and yellow boxes show the layers that were entrained and detrained respectively each hour. Once the vertical and horizontal dimensions of the process analysis box were determined they were then entered into the process analysis tool. The PAT generated two excel files representing the model’s physical and chemical processes occurring within the box. These results will now be discussed.

Results

Northern Analysis Region

Meteorological conditions played a large role in transporting pollutants across box boundaries. Figure 11 shows a graph of horizontal and vertical flows within the process analysis box. The fraction of the box advected per hour is represented on the y-axis and hours within the simulation day on the x-axis. In the morning hours there is a net horizontal flow into the box resulting in pollutants being advected vertically out. In the late morning this phenomena is reversed and pollutants are being advected vertically into the box through the afternoon and night hours. As a



March 15, 2004

result, advection processes and not diffusion processes, dominate the vertical transport of pollutants such as ozone.

The PAT shows that the model contained an abundant amount of NO_x. This conclusion is evident in several plots that are generated by the tool. Figure 12 represents the VOC to NO_x ratios for the process analysis box. One set shows the ratio based on cell concentrations while a separate set is based on cell emissions. It is clear by these graphs that the ratios are well within the VOC limited region. The modeled VOC/NO_x ratios are consistently higher than the inventory ratios because the average lifetime of VOC tends to be longer than for NO_x. In other words, the model tends to accumulate VOC more than NO_x. This difference shows the importance of comparing observed VOC/NO_x ratios to modeled, rather than inventory ratios. The ratios observed in this region were in the range of 2-6. An efficient, reactive VOC/NO_x ratio is typically in the 6-8 range.

A percent nitrogen composition of the process analysis box, shown in Figure 13, shows a high percentage of NO₂ throughout the simulation day. Additionally, NO is present even late in the simulation day suggesting a VOC limited atmosphere. Figure 14 shows the time series plot of NO₂ and O₃ that is a characteristic output of the process analysis tool. The majority of NO₂ is produced chemically in the early morning hours coinciding with the peak NO emissions. The model concentrations show good agreement with ground monitor stations suggesting a reliable NO_x inventory. In addition, the ozone concentrations in this box are also in agreement with ground measurements.

The characteristics of the VOCs that are available in the atmosphere are predominantly low-reactive paraffins. Figure 15 shows the volatile organic compound percent composition of the process analysis box based on cell emissions and cell composition as a function of time. Nearly 70-75% of the cell VOC composition is made up of paraffins with a very small percentage of highly reactive volatile organic carbons such as ethylene or olefin. Cell emissions show a large daytime biogenic isoprene emission due to the inclusion of the state park in the PAB. However, isoprene is not evident in the cell composition as this is a highly reactive compound with a short atmospheric lifetime. This is especially true in a radical limited atmosphere that is apparent in this scenario. For this region there were limited measured data to confirm the model's VOC inventory. The Bethel Island (BTI) station did provide ground VOC data. However, this data was only taken as three hour averages and for a limited number of VOCs. Figure 16 shows the olefin graph with the three hour averaged observed data. The model under predicts the amount of olefins in the atmosphere at each time interval. In Figure 17 the ALD2 observations, a classification of aldehydes, also show an under prediction by the model suggesting inadequate capturing of the full atmospheric VOC chemistry. It is important to note that some olefins are also classified as ALD2 by the chemical mechanism. Therefore, it is unclear whether an under representation of reactive olefins in the emission inventory or lack of chemistry was the reason for the low ALD2 predictions.

The majority of reactive VOCs reacting in this box are predominately isoprene molecules. There are inadequate amounts of VOC available to generate large amounts of ozone chemically. This is evident in all the cycle diagrams that are output by the process analysis tool. The chemical NO_x cycles, radical cycles, chemical production of ozone, and percentage of OH reacting with VOC are all at insufficient levels. Figure 18 is a diagram showing an ozone production diagram including radical and NO_x cycles in the northern source region for local hours 8-18. In the diagram the upper left corner shows the concentration of new OH radicals from the photolysis of



March 15, 2004

aldehydes and O₃, 23.47 ppb. These new radicals are then mixed with recreated OH to show the total number OH that reacted, 74.26. P_{OH} shows the percentage of the OH that reacted with VOCs, .684, the remainder reacting into termination products. 3.165 is the OH cycle number, and 1.58 NO molecules were reacted into NO₂ per VOC. The amount of NO₂ resulting from these reactions, 99.584 ppb, plus new NO₂, 18.58 ppb, are input into the lower NO cycle box. The NO cycle box is similar to the OH box with P_{NO} of .527 and a 2.115 value for the NO cycle. Finally, the NO₂ is photolyzed and O₃ is generated at a ratio of ([O(³p)]/[NO₂]hv) of .873. As a result, 56.23 ppb of O₃ are produced chemically. Some of that O₃ is then photolyzed to produce new OH radicals. The remaining O₃ is added with the various transport and deposition processes to give a final ozone concentration of 74.41 ppb.

From the diagram only 60.83 ppb of VOC reacted with OH radicals. As a percentage of the total OH radicals reacted, only 68% were with VOCs leading to a diminutive radical cycle of 3.165. A more reactive mixture would show cycles in excess of 4. The NO cycle in this region is 2.115, whereas a more reactive mixture would be approximately 3. Figure 19 shows the distribution of the final NO_y in the northern source region for hours 8-18. Thirty-three percent (33%) of the final NO_y remains as NO₂, indicative of a lack of radicals to chemically react with the pollutant.

Figure 20 shows the model ozone concentrations and processes for the northern ozone region. Observed ozone data was recorded at three locations within this PAB. Overall, the model was able to match the peaks recorded there, but did not maintain high ozone concentrations for as long as the rural site at KRE indicates. More than half the ozone remaining in the box at 6 PM is from vertical advection.

Southern Analysis Region

Figure 21 shows a graph of horizontal and vertical flows within the process analysis box for the southern ozone region. The fraction of the box advected per hour is represented on the y-axis and hours within the simulation day on the x-axis. In the morning hours there is a net horizontal flow out of the box resulting in pollutants being advected into the box vertically. This continues for the majority of the day except for a few hours in the late evening when this phenomenon is reversed and pollutants are being advected vertically out. As a result, the advection processes and not diffusion processes dominate the vertical transport of pollutants such as ozone. This could be occurring due to the channeling of wind as a result of the mountainous terrain. The model was unable to match the ozone peaks recorded there. This suggests that the atmosphere did not possess the necessary chemical production needed to get large levels of ozone concentrations. The following will detail the chemical processes that may have caused this under prediction.

The southern ozone region exhibited many of the same chemical characteristics as the northern source region. The process analysis tool again showed that the model contained an abundant amount of NO_x in the PAB. A percent nitrogen composition of the box, shown in Figure 22, shows a high percentage of NO₂ throughout the simulation day. Additionally, NO is present even late in the simulation day suggesting a VOC limited atmosphere. However, the VOC inventory in this area contained more olefins resulting in a more reactive mixture. Figure 23 represents the VOC to NO_x ratios for the process analysis box. It is evident by these graphs that the ratios are in the VOC limited region; however, the ratios are higher than in the northern source region. The reason for the change in reactivity is a shift in characteristics of the VOCs



March 15, 2004

that are available in the atmosphere. The majority of VOCs are still predominantly low-reactive paraffins, but there is an increase in reactive olefins. Figure 24 shows the volatile organic compound percent composition of the process analysis box based on cell emissions and cell composition as a function of time. A large percentage of VOCs in the cell composition are still paraffins. In contrast to the northern source region, a slight increase in the percentage of the composition of reactive olefin and toluene is evident. Cell emissions show a large daytime biogenic isoprene emission due to the inclusion of natural areas in the process analysis box.

For this region there were observed data from one ground monitoring station that was used to help confirm the model's VOC inventory. The Sunol (SUNO) ground station in the southwest area of the domain provided speciated VOC data at one hour averages for a limited number of VOCs. Observed ethylene values were reasonably consistent with model values. Figure 25 shows the olefin graph with the observed data. The model under predicts the amount of olefins in the atmosphere at each time interval. Figures 26 and 27 also show model under predictions of observed toluene and xylene concentrations. In Figure 28 the ALD2 observations, a classification of aldehydes, illustrate an under prediction by the model suggesting inadequate capturing of the full atmospheric VOC chemistry. Again, it is important to note that some olefins are also classified as ALD2 by the chemical mechanism. Therefore, it is unclear whether an under representation of reactive olefins in the emission inventory or a lack of chemistry was the reason for low ALD2 predictions.

The majority of reactive VOCs chemically reacting in this box are predominately isoprene molecules. There are inadequate amounts of VOC available to generate large amounts of ozone chemically. This is evident in all the cycle diagrams that are output by the process analysis tool. The chemical NO_x cycles, radical cycles, chemical production of ozone, and percentage of OH reacting with VOC are all at insufficient levels. Figure 29 is a diagram showing an ozone production diagram including radical and NO_x cycles in the southern ozone region for hours 8-18. From the diagram only 57.93 ppb of VOC reacted with OH radicals. As a percentage of the total OH radicals reacted only 70% were with VOCs leading to a diminutive radical cycle of 3.409. When compared to the northern source region there is a smaller amount of VOCs reacted with OH radicals, but the radical cycle is larger. This is indicative of the slightly more reactive VOC mixture in the southern region's atmosphere. The NO cycle in this area is still an unreactive value of 2.351. Figure 30 gives the ozone yield per VOC species for the northern source region and southern ozone region. The more reactive atmosphere in the south gives a slightly higher ozone yield for most VOC compounds. Figure 31 shows the distribution of the final NO_y in the southern ozone region for hours 8-18. Fifty percent (50%) of the final NO_y remains as NO₂ indicative of a lack of radicals with which to chemically react.

Figure 32 shows the model ozone concentrations and processes for the southern ozone region. Observed ozone data was recorded in the urban Livermore area. The model was unable to match the peaks recorded there. This suggests that the atmosphere did not possess the necessary chemical production needed to get large levels of ozone concentrations.

Conclusions

In both regions vertical advection played an important role in the transport of pollutants across the boundaries of the process analysis boxes. This can be attributed to the heterogeneity of the terrain under analysis. These differences in terrain account for a wide range of mixing and



March 15, 2004

vertical advection. To minimize these differences and correctly capture the mixing height, the process analysis boxes could be split into two adjoining boxes. For example, in the northern source region, one box would cover the source region along the Sacramento River and the second box the ozone region over the state park. This improved methodology would enhance model comparisons with the Bethel Island (BTI) ground monitor. A smaller process analysis box over the Sacramento River area would exclude the state park and minimize the dilution effects of including an area with a lack of pollutant emissions. This would also separate the anthropogenic from the biogenic VOCs clarifying the characteristics of the atmospheric chemistry. A similar approach could be applied in the southern ozone region.

Similar chemical characteristics were evident in the atmospheres of both regions. The process analysis tool determined that the modeled atmosphere is NO_x rich and VOC limited. The composition of the VOC that was available in the atmosphere was predominantly low-reactive paraffins. Since both areas incorporated natural terrain a significant amount of isoprene was emitted during the day into both process analysis boxes. Nevertheless, there were still inadequate amounts of reactive VOC available to generate large amounts of ozone chemically. This is evident in all the cycle diagrams that are output by the process analysis tool. The chemical NO_x cycles, radical cycles, chemical production of ozone, and percentage of OH reacting with VOC were all at insufficient levels. The southern region was slightly more reactive and had higher radical cycles due to the inclusion of more olefins. This still fell far below the levels needed to reach observed ozone peaks in the Livermore area. In the full gridded CAMx model the areas of high ozone concentration occurred over natural areas where sufficient isoprene emissions mixed with pollutants from the urban plume.

The low concentrations of reactive VOCs in the atmosphere were not consistent with observed VOCs. The Bethel Island (BTI) station in the northern source region provided ground VOC data, but only at three hour averages and for a limited number of VOCs. In this region the model under predicts the amount of olefins and aldehydes in the atmosphere by a factor of 5. In the southern ozone region the Sunol (SUNO) ground station provided speciated VOC data at one hour averages for a limited number of VOCs. Similarly to the northern region, the model under predicts the amount of olefins, toluene, xylene, and aldehydes in the atmosphere by as much as a factor of 5. The model's inability to generate the observed concentrations of aldehydes could be evidence that the model is not fully capturing all the atmospheric VOC chemistry. However, some reactive olefins are also classified as ALD2 which points to an underrepresented emission inventory. Observed ethylene concentrations were consistent with model values. This suggests that the meteorology of the model has been properly simulated and is not the cause of the OLE/ALD2 discrepancies. Further investigation is needed to explore the discrepancies found in the OLE emission inventory.

The strongest possibility for the low reactivity could be the lack of total VOC and/or the improper speciation of the general anthropogenic emission inventory. As a matter of comparison, in the Houston Texas air shed VOC under predictions were attributed to industrial upset events. Large uncertainties in the number, magnitude, and duration of these upset events exist within the photochemical grid model's emission inventories. Observed data from aircraft taken during the Texas Air Quality Study 2000 has reported olefin concentrations of nearly 25 ppb downwind from an industrial upset event (Vizuete *et al.*, 2004). The inclusion of such upsets (if they indeed occurred) would shift the reactivity of the VOC composition and yield higher ozone production in the San Francisco Bay Area.

March 15, 2004

REFERENCES

- ENVIRON, 2004. CAMx Users Guide, v4.00. www.camx.com.
- Jeffries H., T. Keating, and Z. Wang, 1997. "Integrated Process rate analysis of the effect of nitrogen oxides emission height on peak ozone concentration predicted by the urban airshed model." Department of Environmental Sciences and Engineering, School of Public Health, The University of North Carolina - Chapel Hill, <http://airsite.unc.edu>. Contract No. 5094-250-3069.
- Russell A. and Dennis R., 2000. "NARSTO critical review of photochemical models and modeling." *Atmospheric Environment*, Volume 34, Issues 12-14, Pages 2283-2324.
- Seinfeld J. and S. Panids, 1998. *Atmospheric Chemistry and Physics*. John Wiley and Sons, Eds.
- Tesche T. W., D. E. McNally, J. G. Wilkinson, H. E. Jeffries, Y. Kimura, C. Emery, G. Yarwood, and D. R. Souten, 2004. "Evaluation of the 16-20 September 2000 Ozone Episode for use in 1_hr SIP Development in the California Central Valley." Report prepared for the California Air Resources Board (AG-90/TS201).
- Tonnesen S., 1995. "Development and application of a process analysis method for photochemical oxidant models." Dissertation, University of North Carolina at Chapel Hill, Environmental Sciences and Engineering, School of Public Health.
- Vizuete W., Y. Kimura, D. Allen, H. Jeffries, 2004. "Ozone formation phenomena in Southeast Texas," manuscript in preparation to be submitted to *Atmospheric Environment*.

Conceptual Model

$$\begin{aligned}
 &\text{Concentration at } t+h \\
 &= \\
 &\text{Concentration at } t \\
 &+ \text{ change due to horizontal transport} \\
 &+ \text{ change due to vertical transport} \\
 &+ \text{ change due to emissions} \\
 &+ \text{ change due to deposition(wet \& dry)} \\
 &+ \text{ change due to chemical production} \\
 &+ \text{ change due to chemical loss} \\
 &+ \text{ change due to phase change}
 \end{aligned}$$

environmental state
environmental state
environmental processes

some changes are positive and some are negative

Figure 1. Conceptual model explaining processes that contribute to changes in pollutant concentrations.

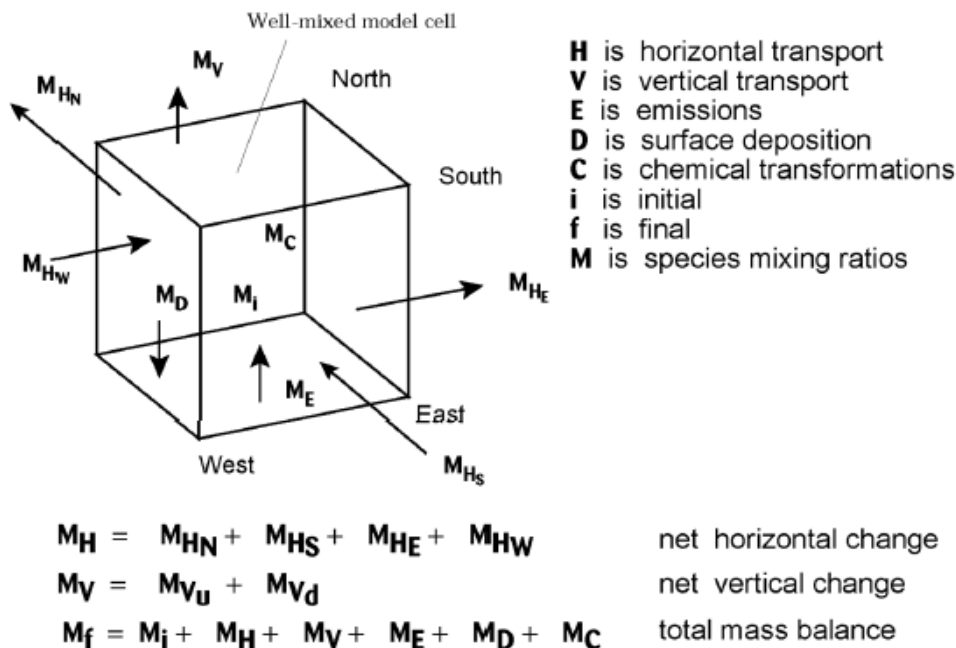


Figure 2. Models are formulated using “well-mixed” chemical reactor cells that hold concentration information and are subject to a collection of processes that modify those concentrations over short time steps.

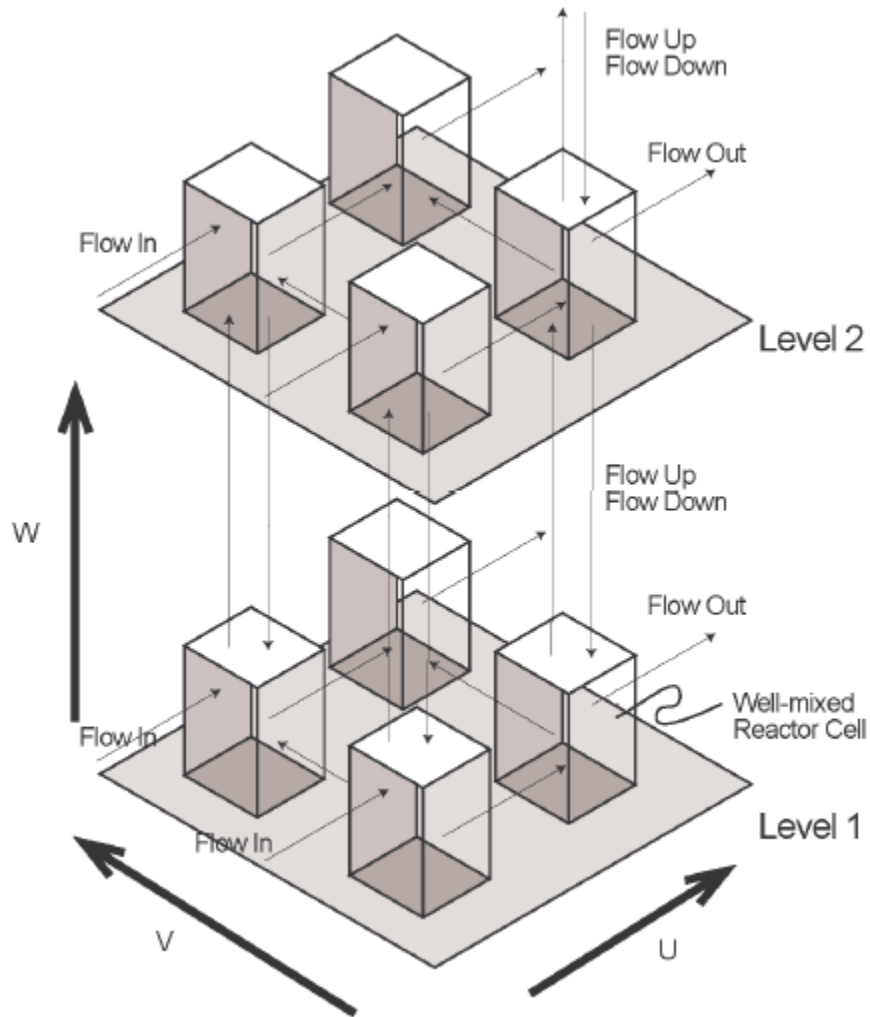


Figure 3. Conceptual drawing of the CAMx grid cell network of many “well-mixed cells” coupled together via cell to cell transport through all faces in common with other adjacent cells. This cell-to-cell transport can either be by advection or by diffusion.

March 15, 2004

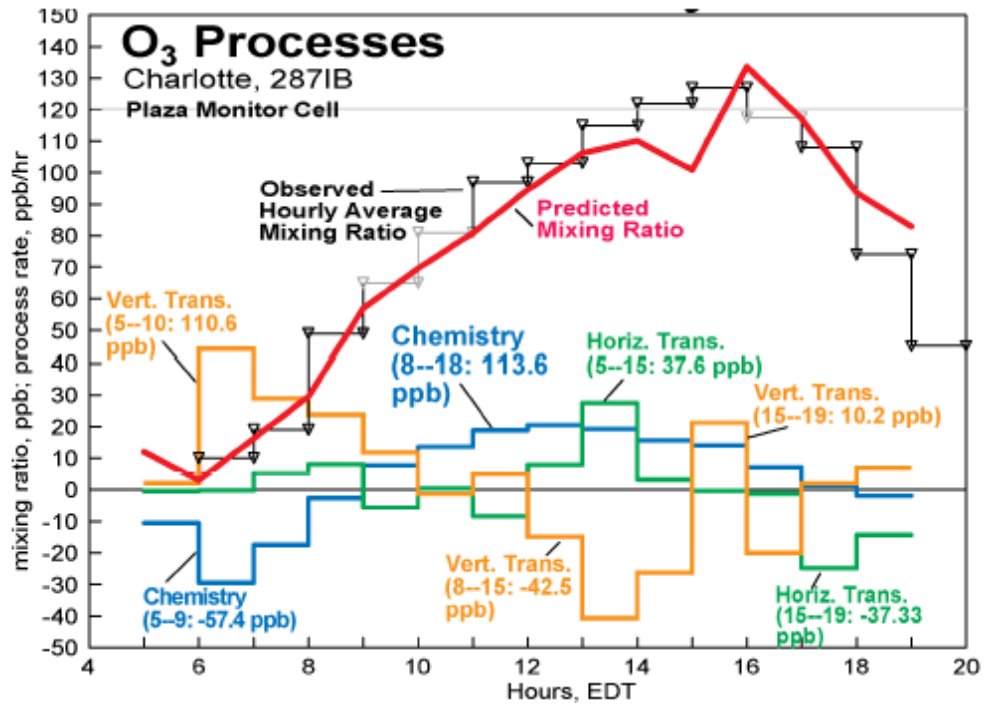
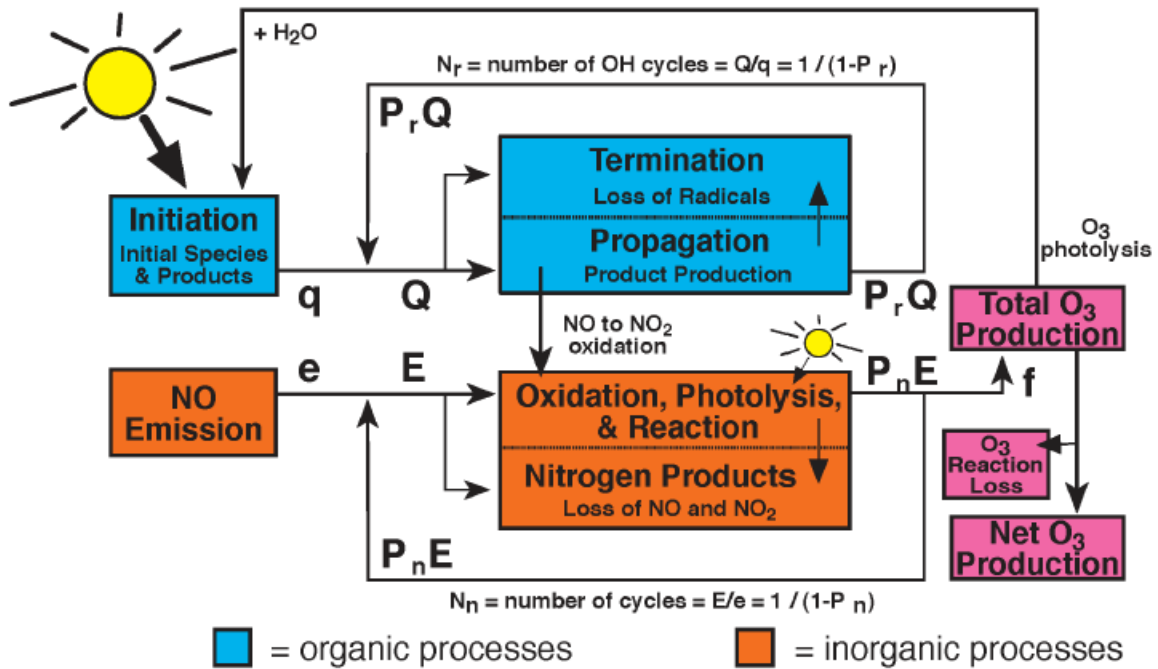


Figure 4. Example Process Analysis time series plot with observed hourly averaged observations.

March 15, 2004



- q = "new OH" radicals produced by photolysis, ppb
- Q = "total OH" radicals reacting, ppb: $Q = q + q P_r + q P_r^2 + \dots = q / (1 - P_r)$
- P_r = OH propagation factor, <1.0 due to termination
- e = "new NO" from emissions, ppb
- E = "total NO" reacting, ppb: $E = e + e P_n + e P_n^2 + \dots = e / (1 - P_r)$
- P_n = NO propagation factor, <1.0 due to termination
- f = net O₃ yield from NO₂ photolysis

Figure 5. Conceptual model of the radical and nitrogen oxides chemical cycles resulting in ozone production.

March 15, 2004

Charlotte 6x6 5-km surface cells, Day 2 287fc 6--19 Hours

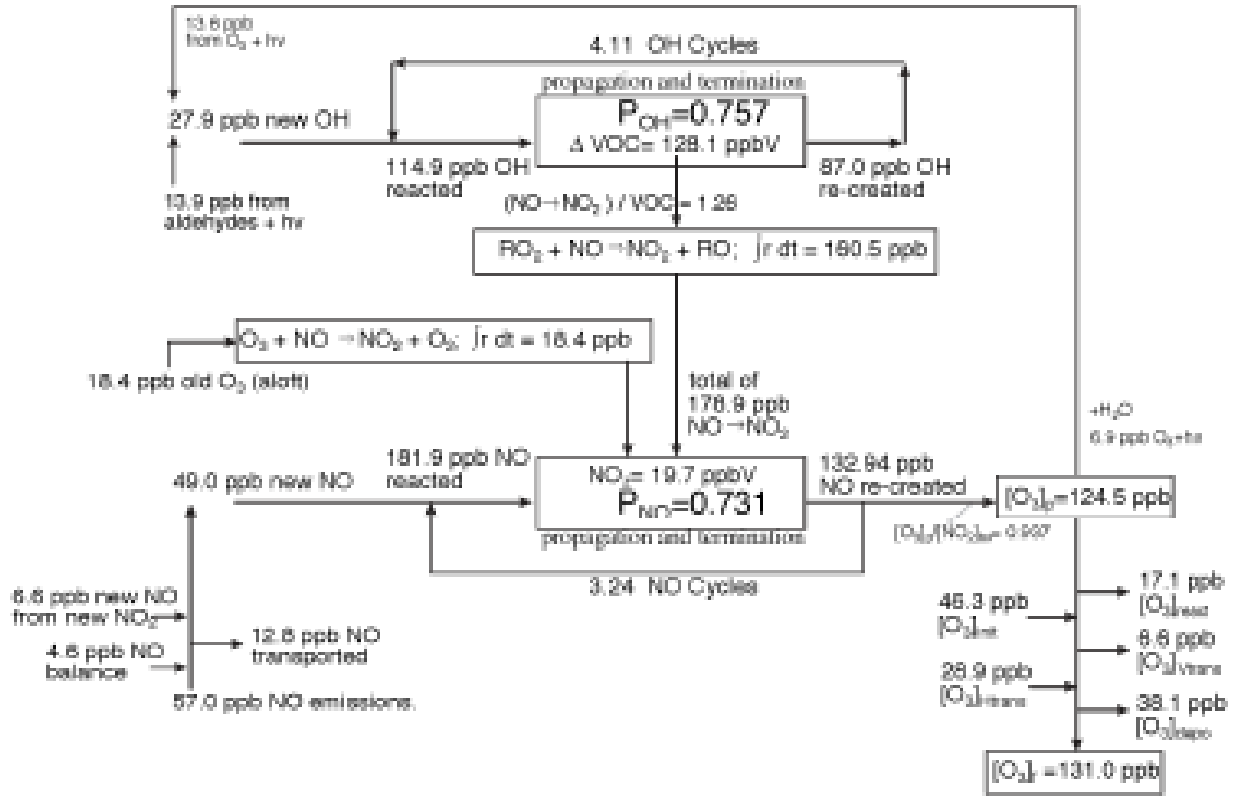
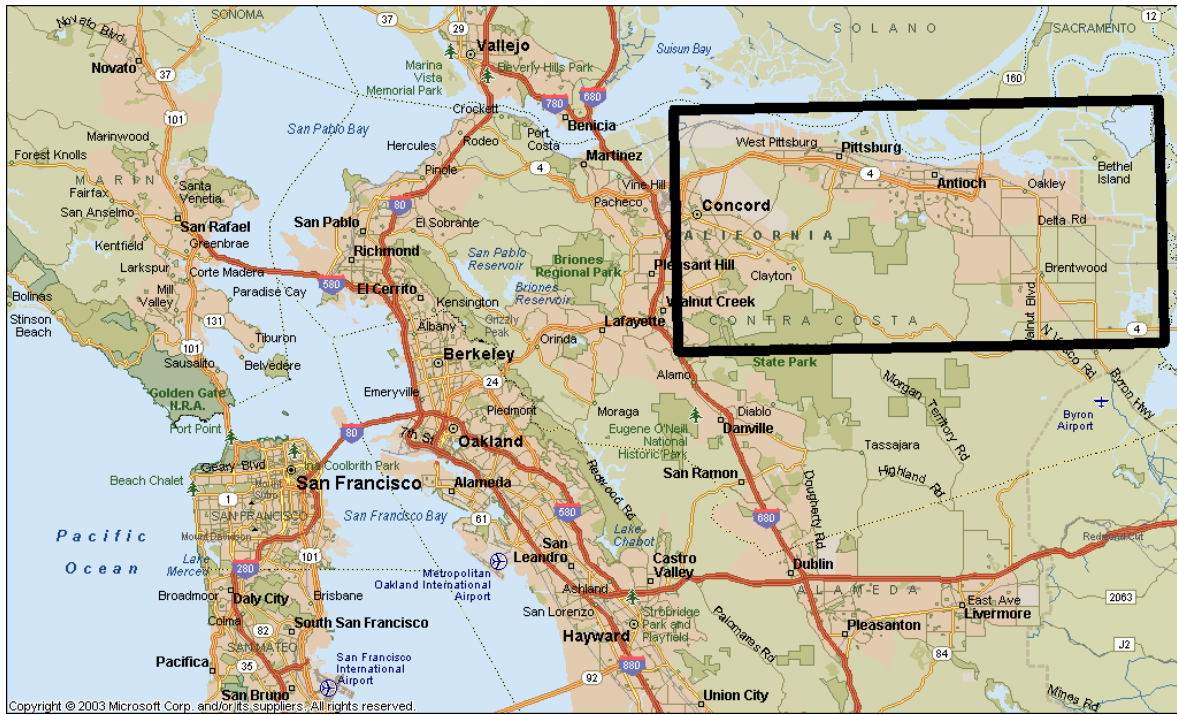


Figure 6. Example of the Process Analysis Radical and Nitrogen Cycles diagram.

March 15, 2004

A



B

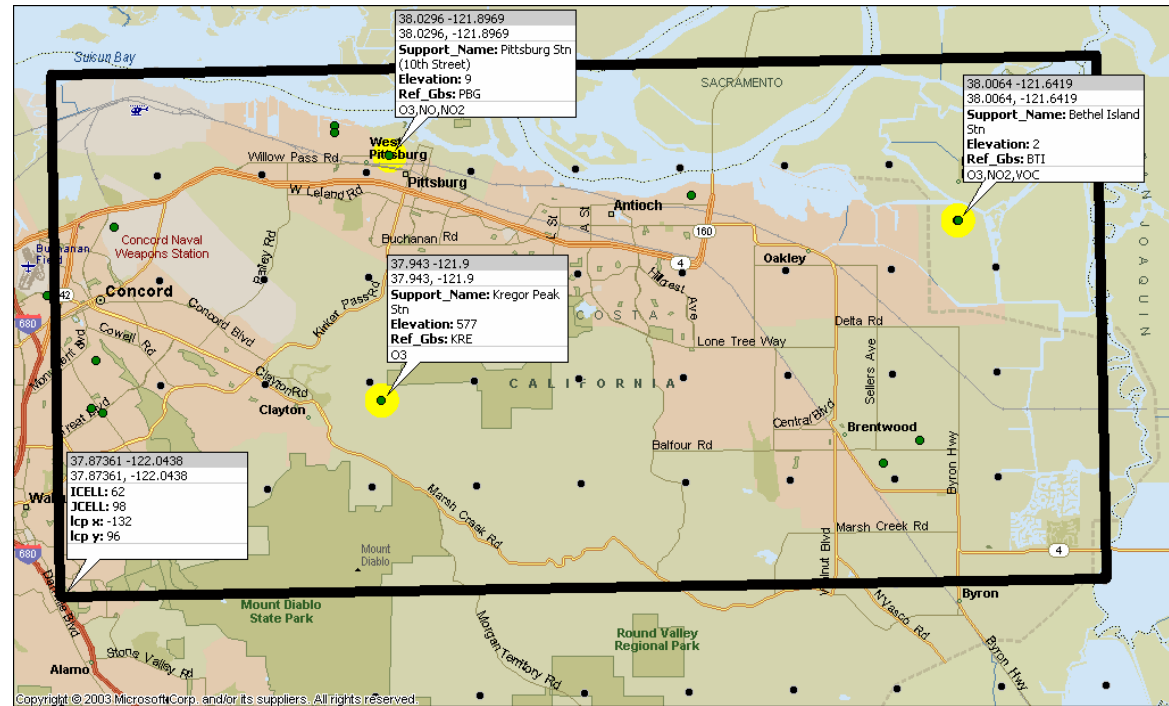


Figure 7. (A) The location of the 640 km² sub-domain, outlined in black, used by the process analysis tool for the northern source region. (B) A close up view of the sub-domain. The black dots represent the lower left corner of the 4 km CAMx grid cells. Observed data was used from the monitor stations that are highlighted on the map.

March 15, 2004

A



B

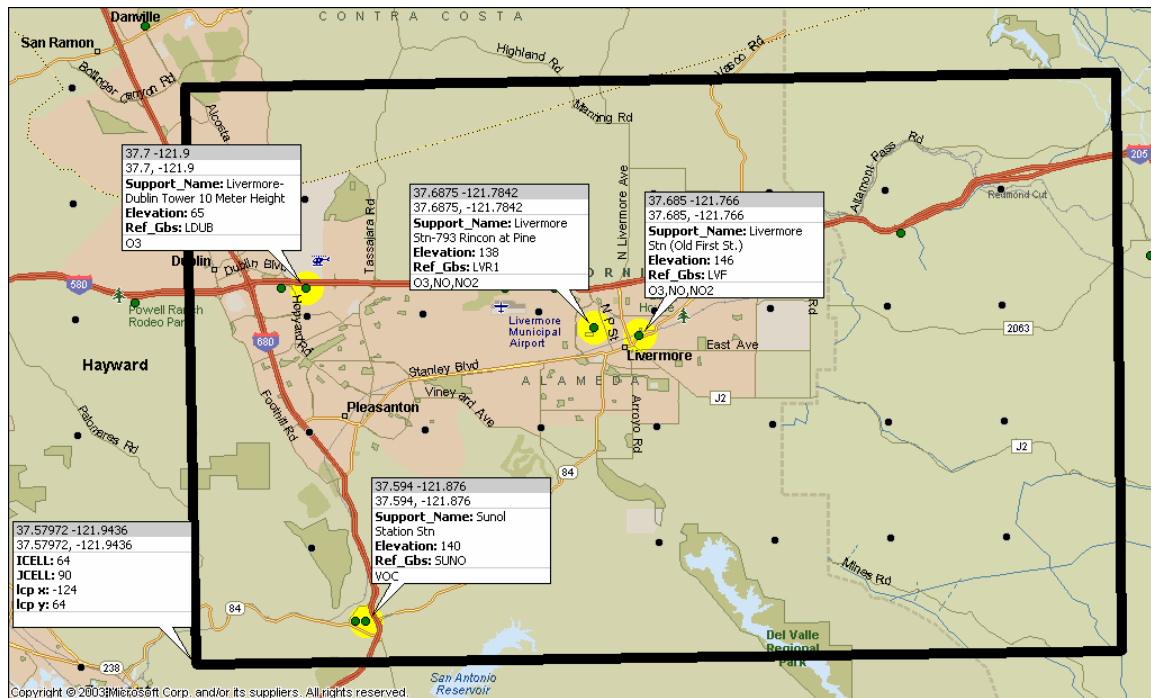


Figure 8. (A) The location of the 640 km² sub-domain, outlined in black, used by the process analysis tool for the southern ozone region. (B) A close up view of the sub-domain. The black dots represent the lower left corner of the 4 km CAMx grid cells. Observed data was used from the monitor stations that are highlighted on the map.

March 15, 2004

Hour 19

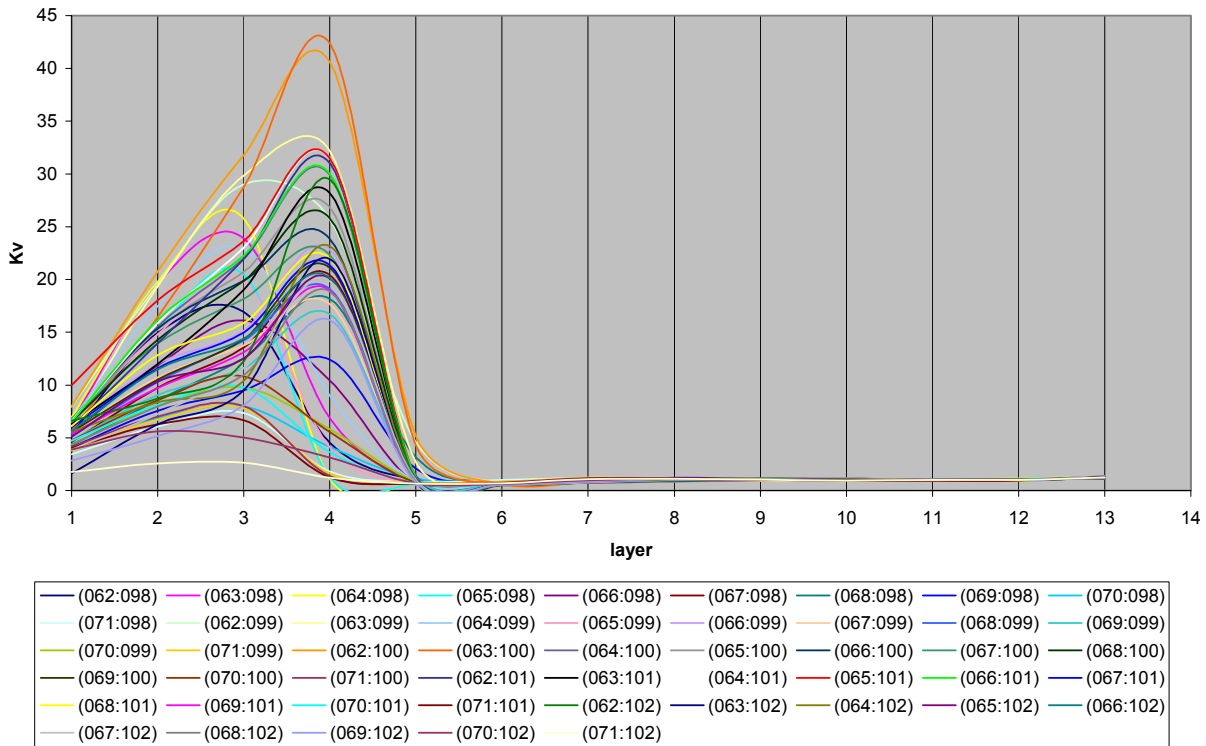


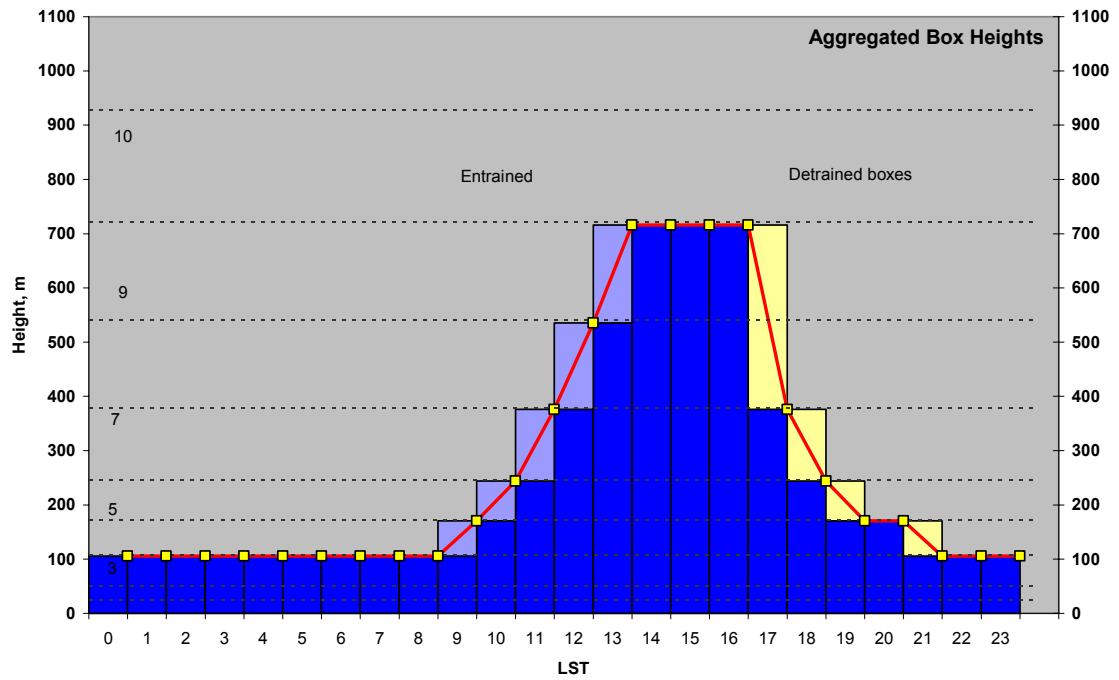
Figure 9. Graph of the Kv parameter versus CAMx model heights for hour 19. Each line on the graph represents a grid cell within the process analysis sub-domain for the northern source region. These values were used to determine the mixing height at each hour within the domain. At this hour the mixing height was determined to extend through layer 5.

March 15, 2004

0731.run8a_pa.ba.sfin-south

camx.000731.run8a_pa.ba.ipr

A



run8a_pa.ba.sfin-north

camx.000731.run8a_pa.ba.ipr

B

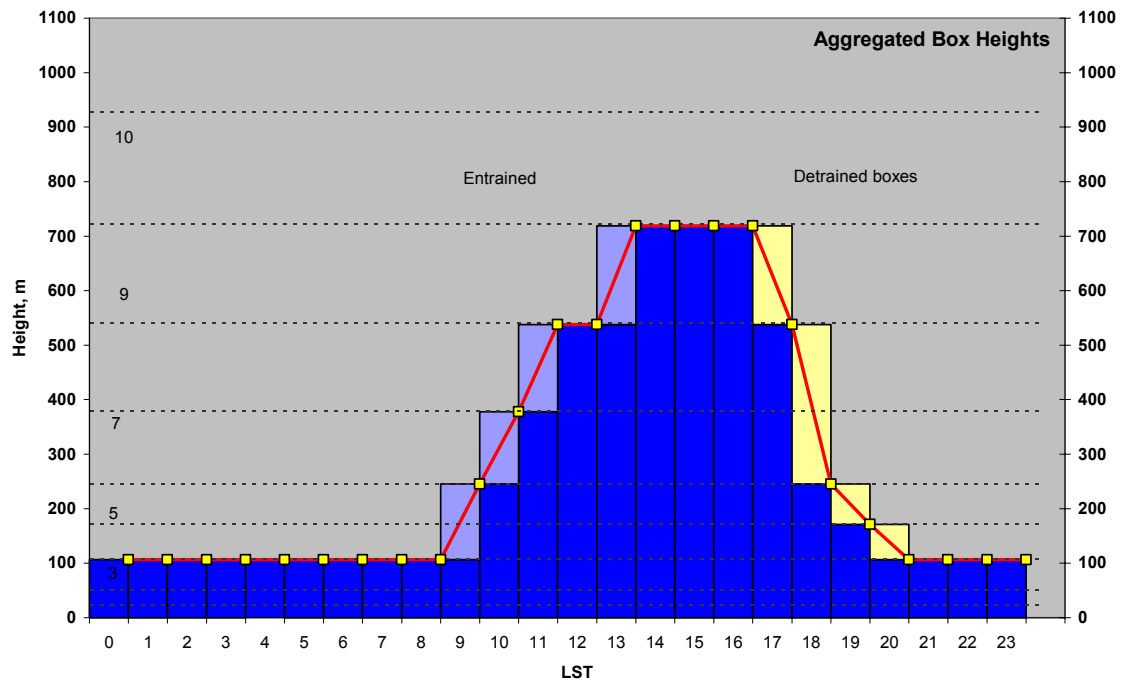


Figure 10. The evolution of the mixing height within the process analysis sub-domain for the (A) northern and (B) southern region. The x-axis represents the hours of the simulation day and the modeling height is shown vertically. The black horizontal grid lines represent the CAMx grid layers and the red line is the mixing height. The light blue and yellow boxes show the layers that were entrained and detrained, respectively.



March 15, 2004

000731.run8a_pa.ba.sfin-north

camx.000731.run8a_pa.ba.ipr

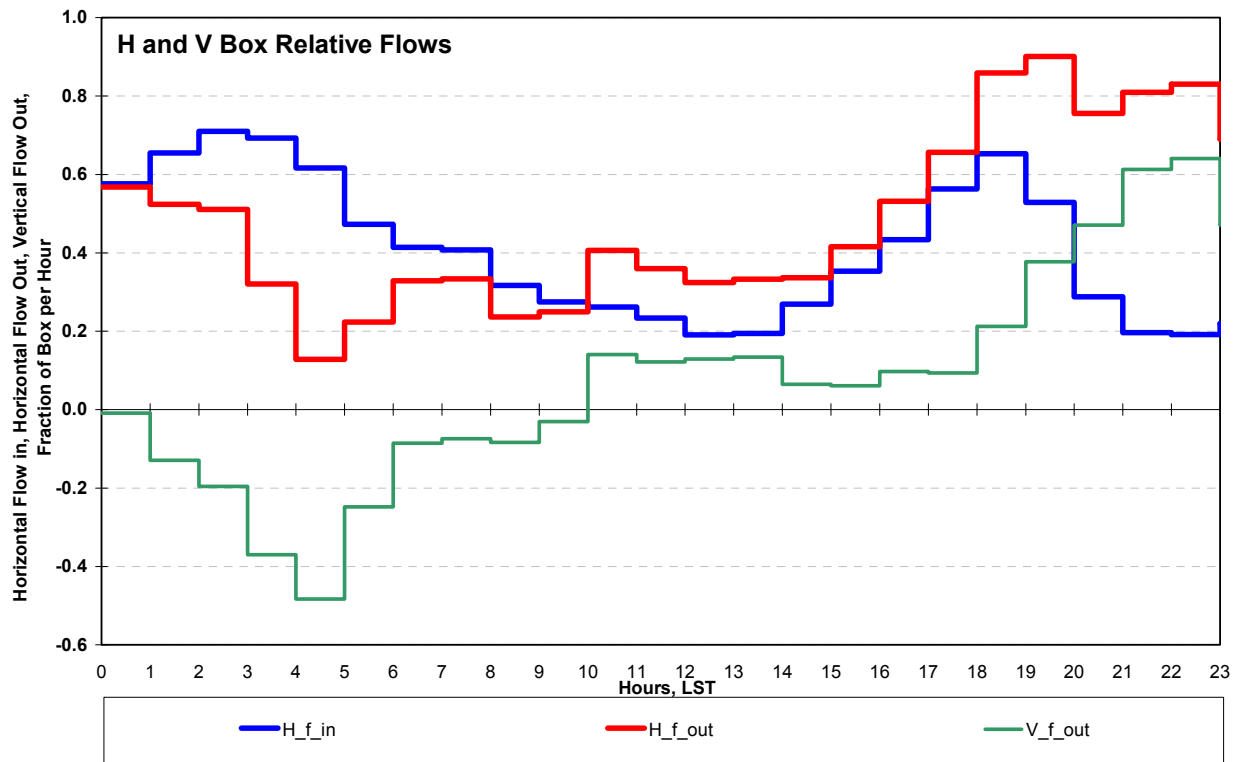


Figure 11. Graph of horizontal and vertical flows within the process analysis box for the northern source region. The fraction of the box advected per hour is represented on the y-axis and hours within the simulation day on the x-axis. In the morning hours there is a net horizontal flow into the box resulting in pollutants being advected out vertically. In the late morning this phenomena is reversed and pollutants are being advected vertically into the box through the afternoon and night hours.

March 15, 2004

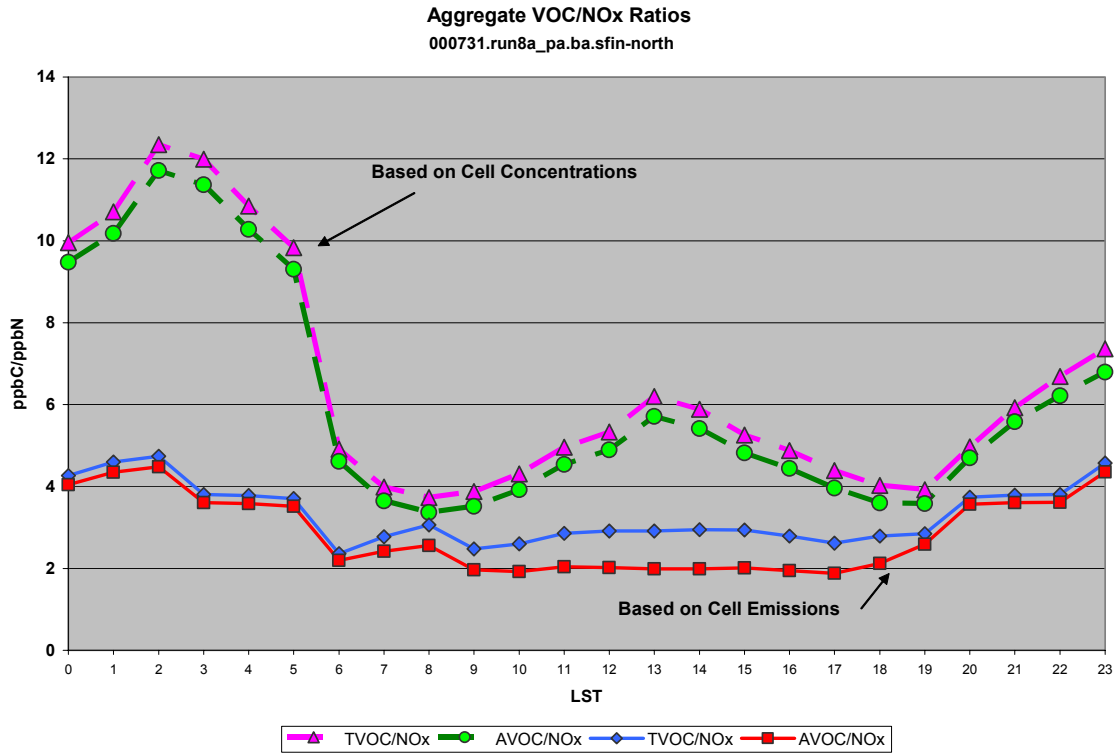


Figure 12. Volatile organic carbon (VOC) to NOx ratios for the process analysis box in ppb C for the northern source region.

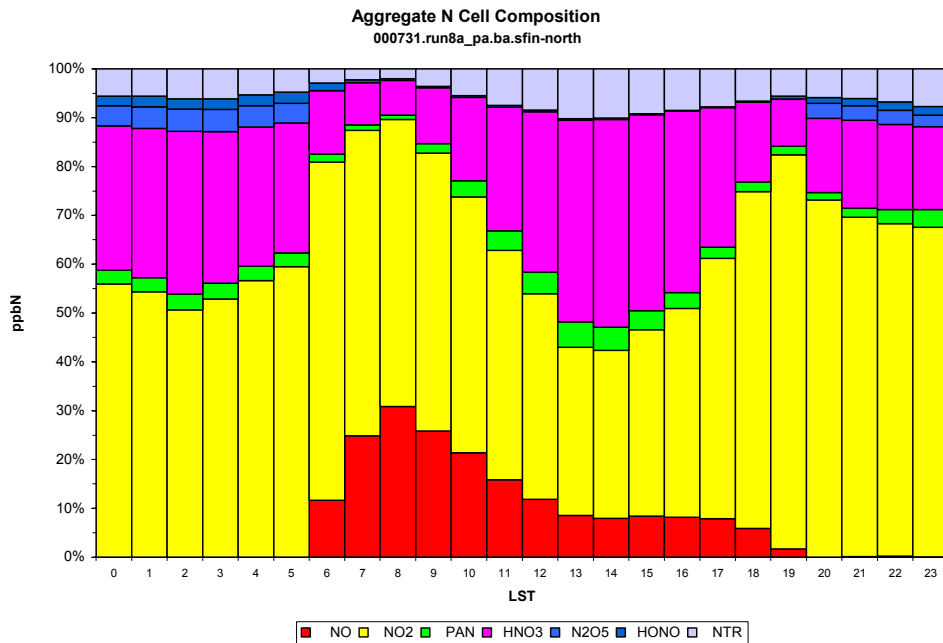


Figure 13. Nitrogen compound percent composition of the process analysis box based on cell concentration as a function of time for the northern source region.

March 15, 2004

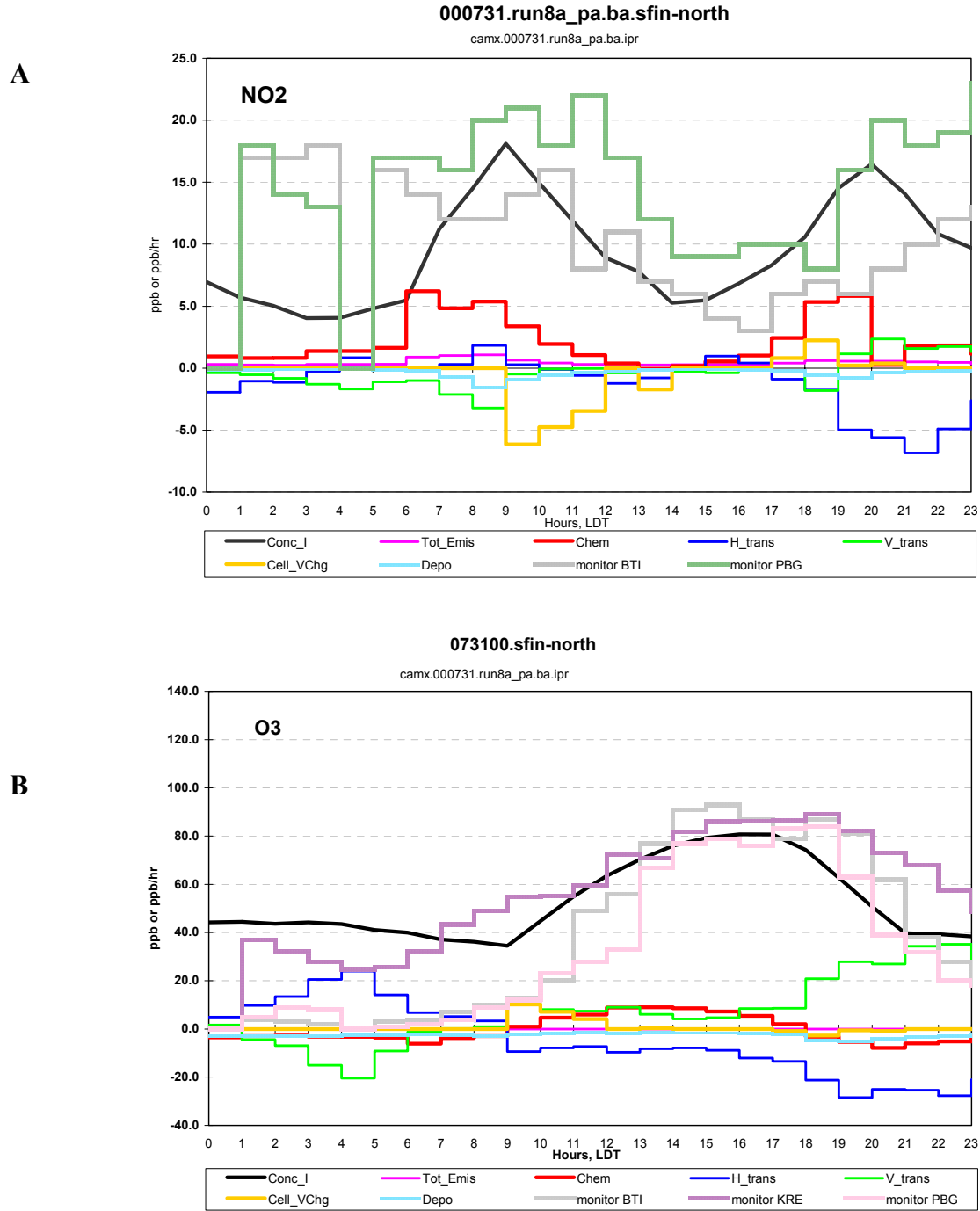
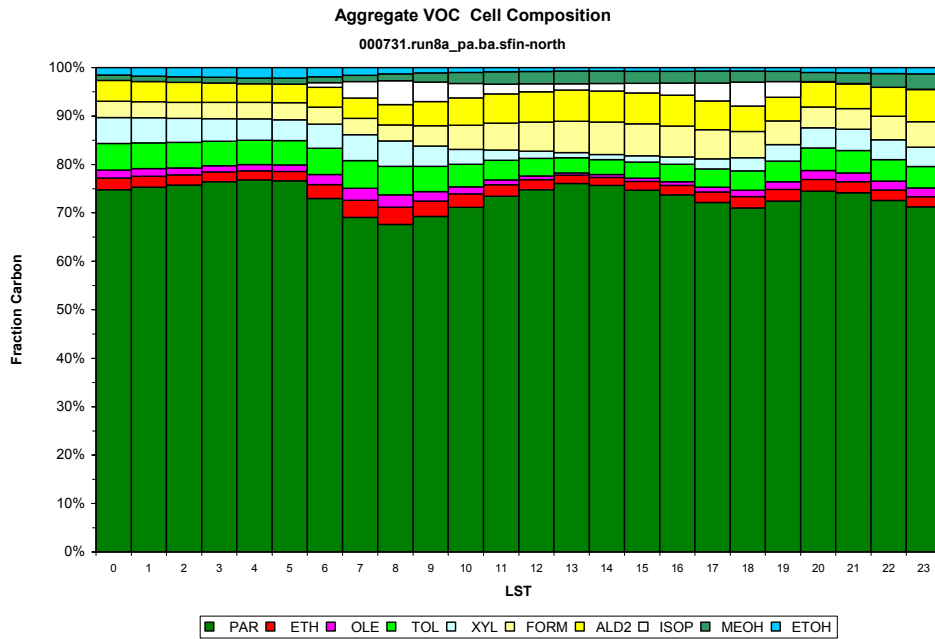


Figure 14. (A) NO₂ and (B) O₃ model concentrations and the processes that contribute to the final concentration for the northern source region.

March 15, 2004

A



B

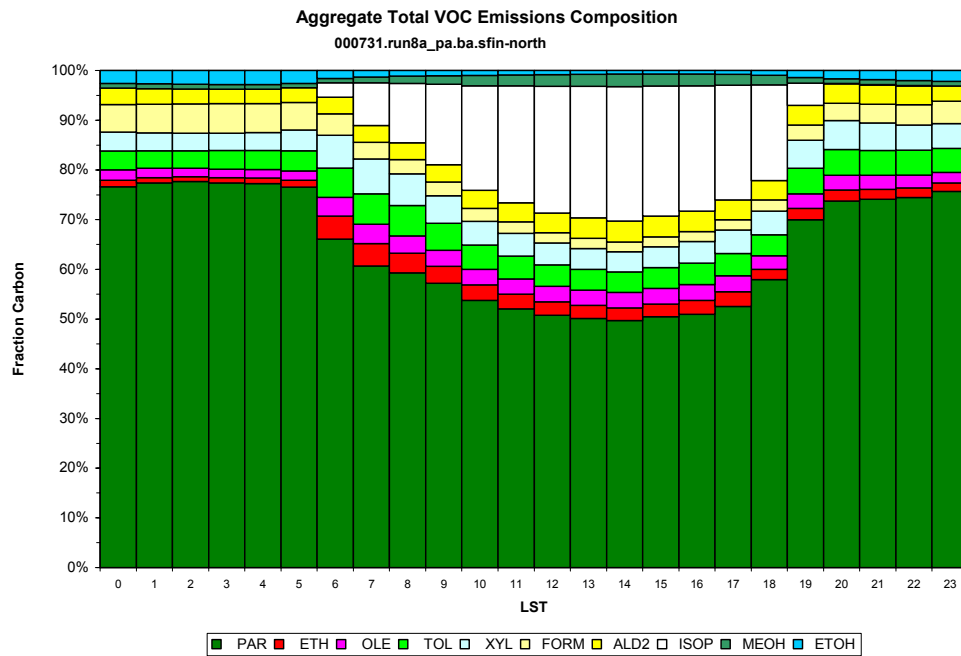


Figure 15. (A) Volatile organic compound percent composition of the process analysis box based on cell emissions and (B) cell concentration as a function of time for the northern source region.

March 15, 2004

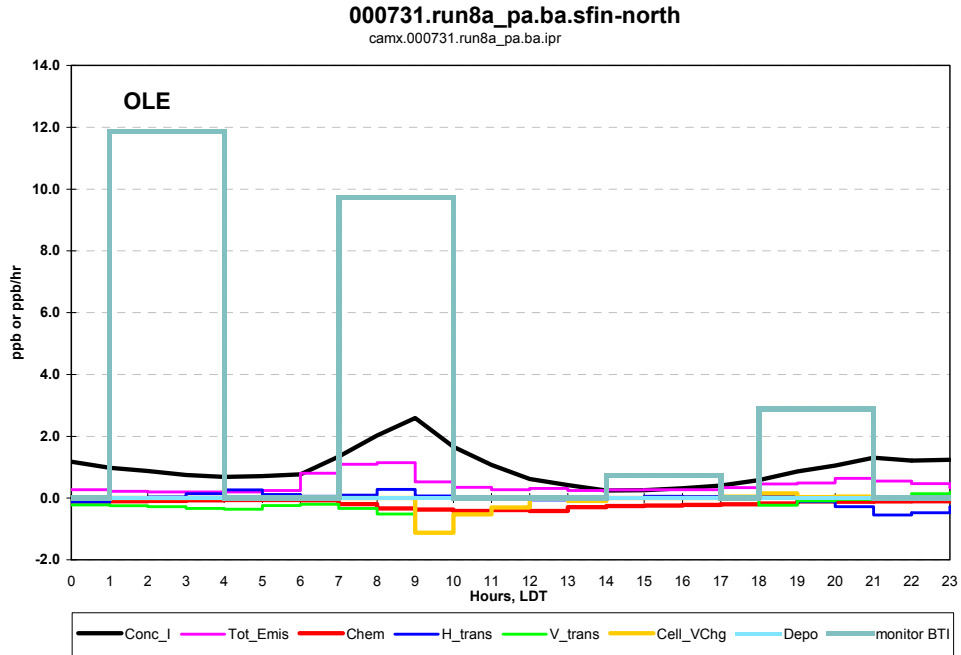


Figure 16. Olefin model concentrations and the processes that contribute to the final concentration for the northern source region. Observed data is shown from the Bethel Island (BTI) monitor station as a three hour average.

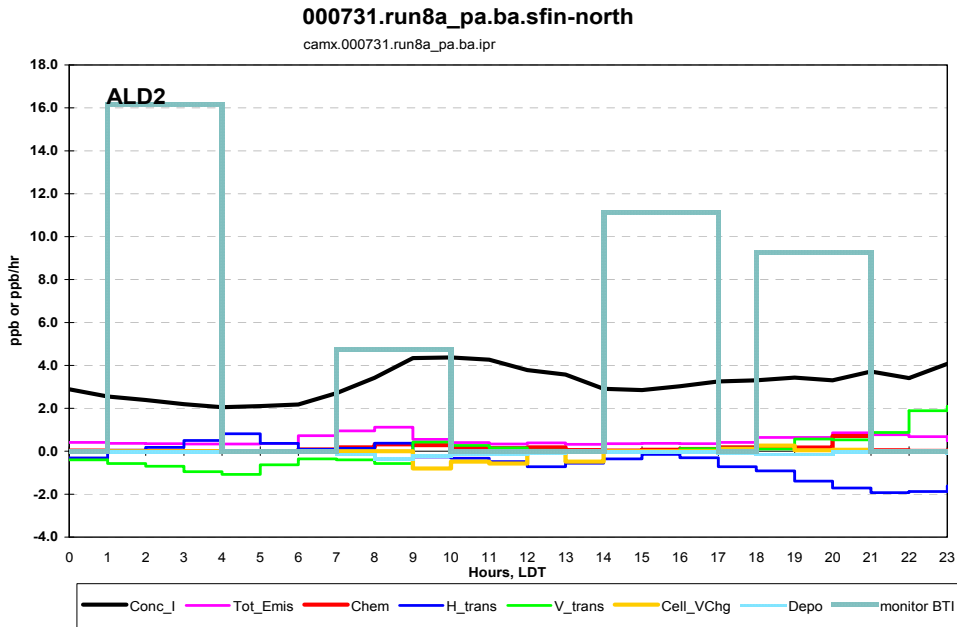


Figure 17. ALD2, a class of aldehydes, model concentrations and the processes that contribute to the final concentration for the northern source region. Observed data is shown from the Bethel Island (BTI) monitor station as a three hour average.

March 15, 2004

camx.000731.run8a_pa.ba.ipr
camx.000731.run8a_pa.ba.irr

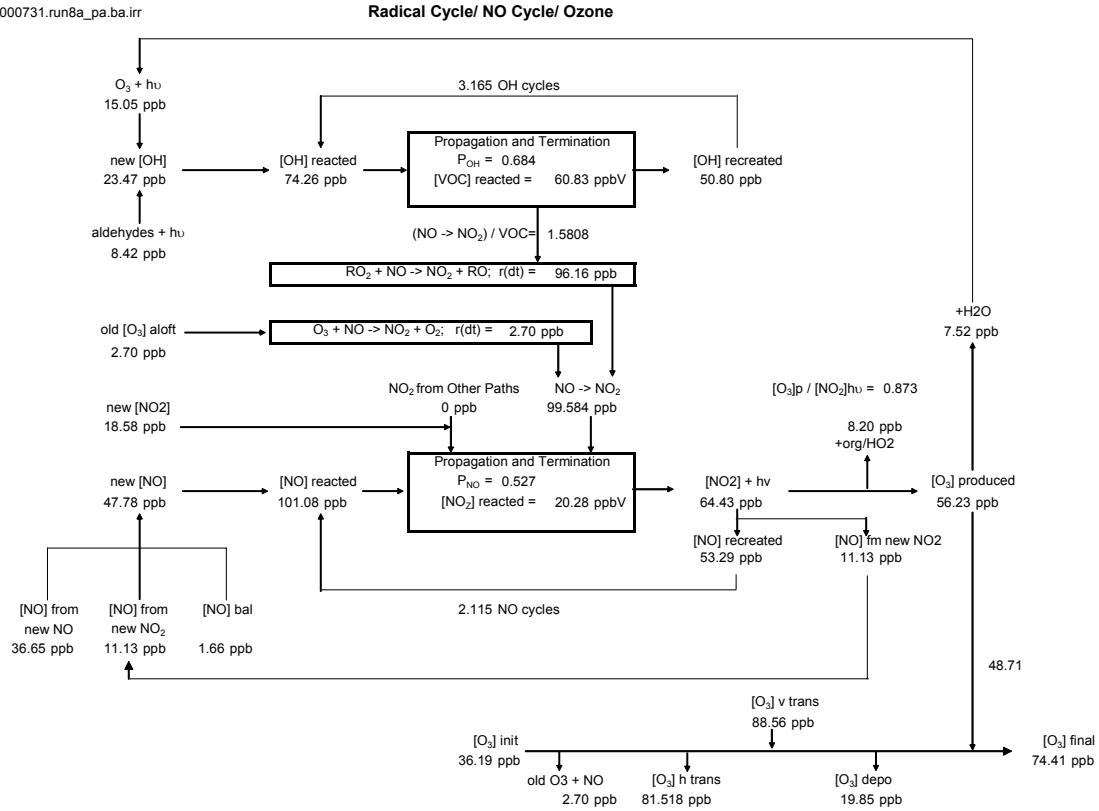


Figure 18. Ozone production diagram including radical and NOx cycles in the northern source region for hours 8-18.

camx.000731.run8a_pa.ba.ipr

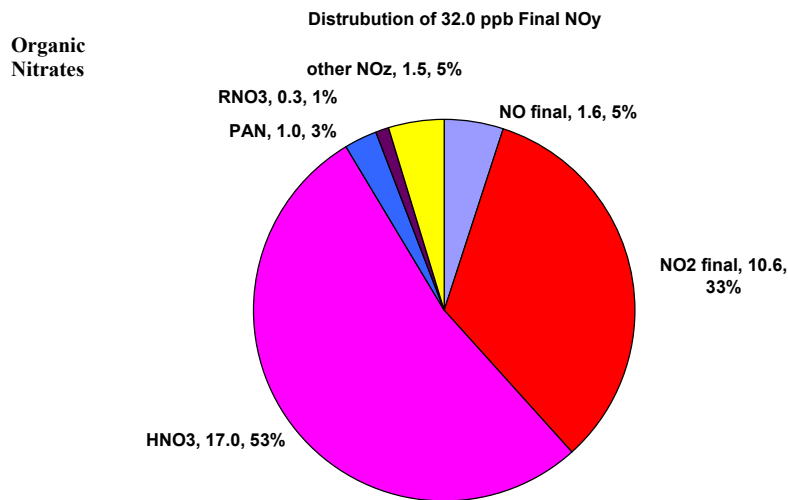


Figure 19. Distribution of the final NOy in the northern source region for hours 8-18.

March 15, 2004

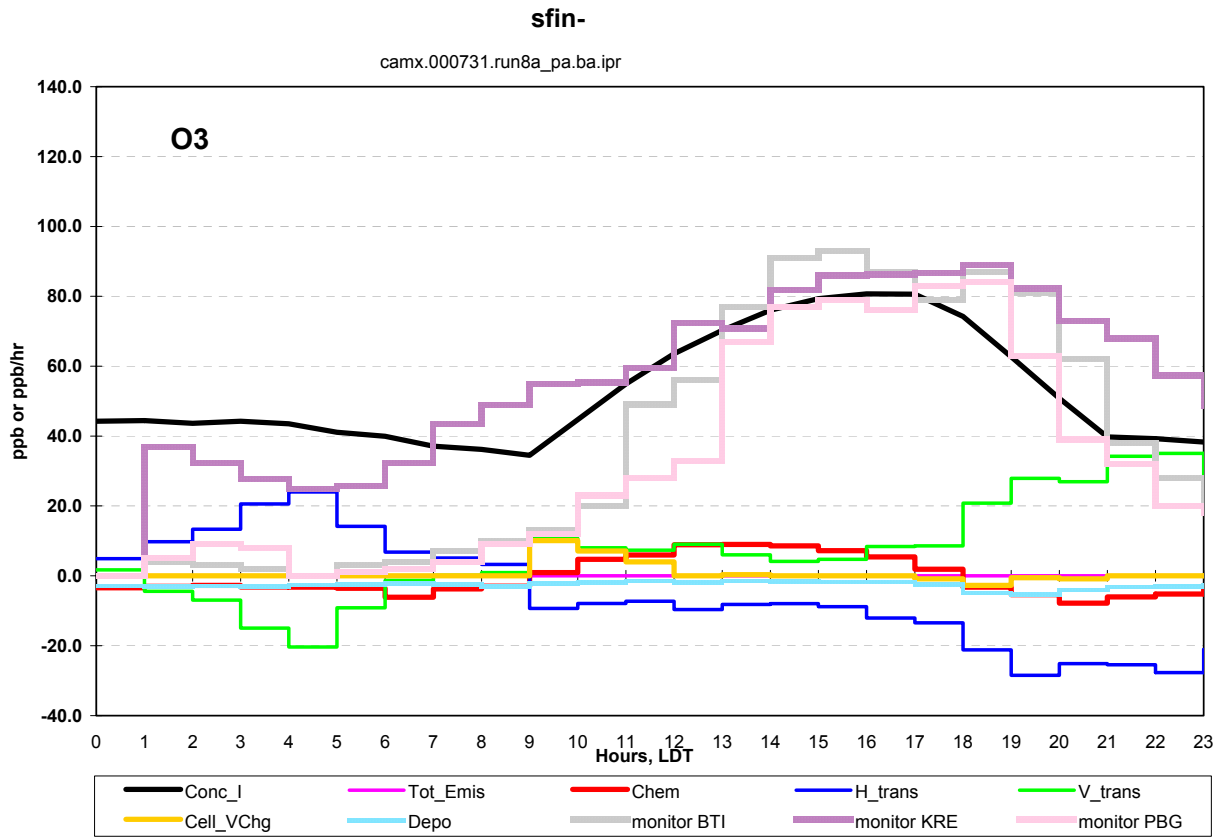


Figure 20. Ozone model concentrations and the processes that contribute to the final concentration for the northern ozone region. Observed data are shown from three monitor stations (BTI, KRE, PBG) as one hour averages.



March 15, 2004

0731.run8a_pa.ba.sfin-south

camx.000731.run8a_pa.ba.ipr

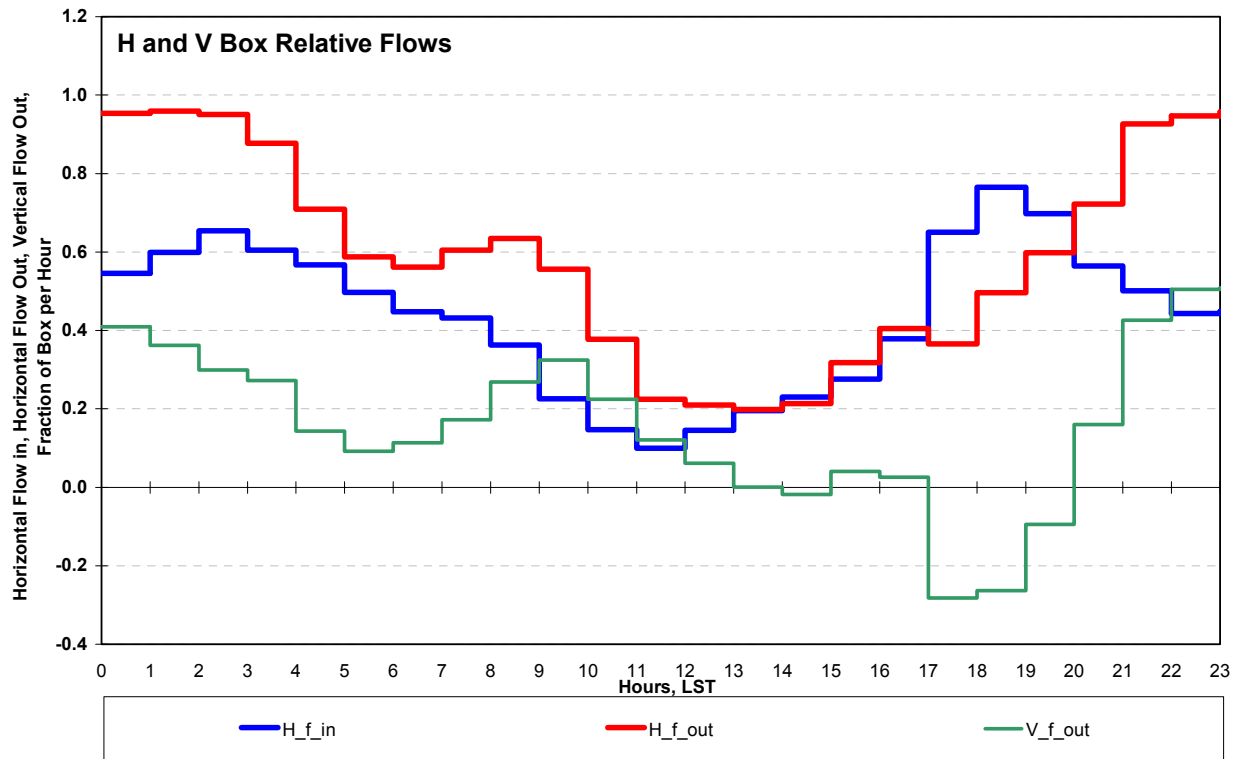


Figure 21. Graph of horizontal and vertical flows within the process analysis box for the southern ozone region. The fraction of the box advected per hour is represented on the y-axis and hours within the simulation day on the x-axis. In the morning hours there is a net horizontal flow out the box resulting in pollutants being advected in vertically. This phenomenon continues throughout the day except for a few hours in the late evening.

March 15, 2004

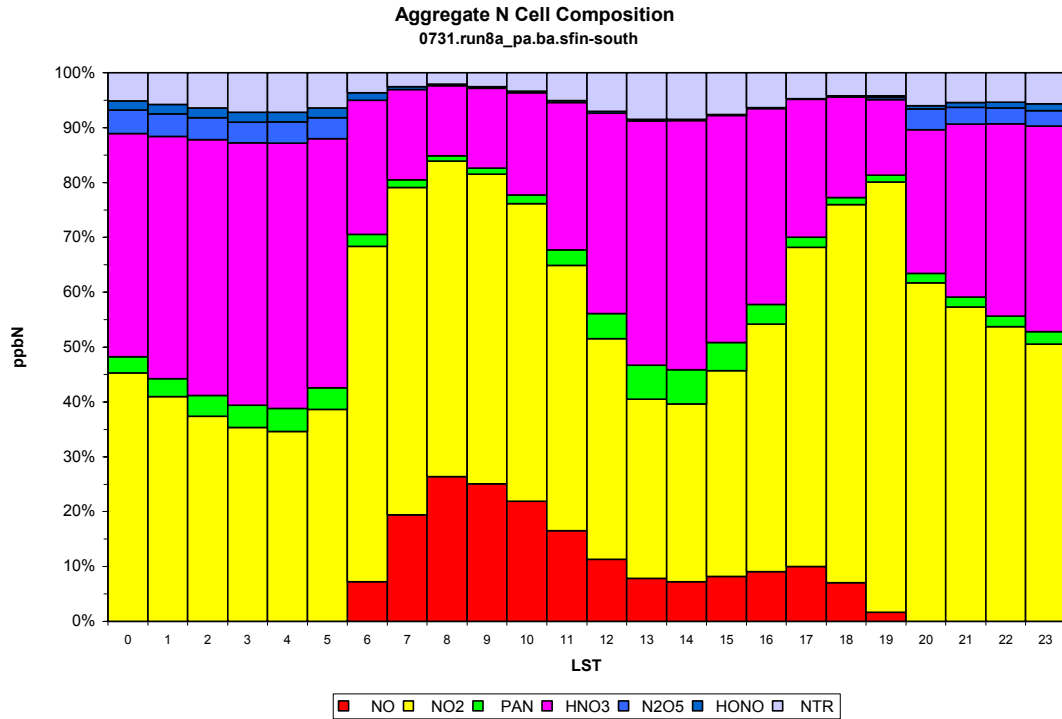


Figure 22. Nitrogen compound percent composition of the process analysis box based on cell concentration as a function of time for the southern ozone region.

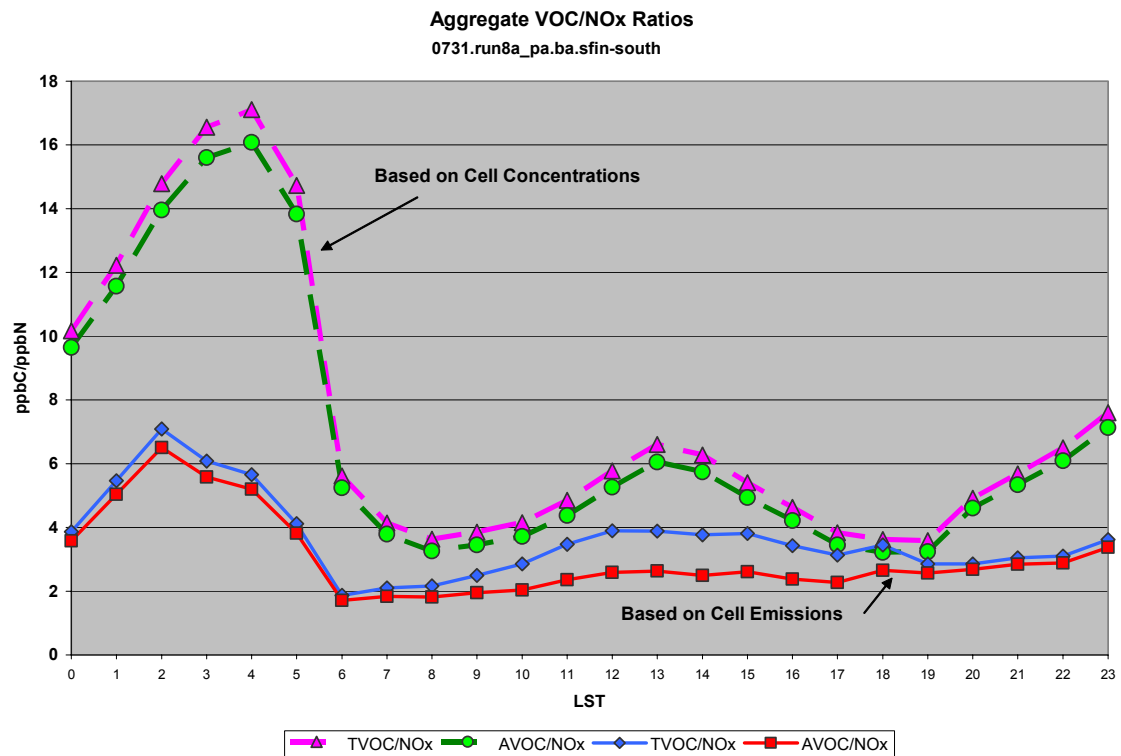


Figure 23. Volatile organic carbon (VOC) to NOx ratios for the process analysis box in ppb C for the southern ozone region.

March 15, 2004

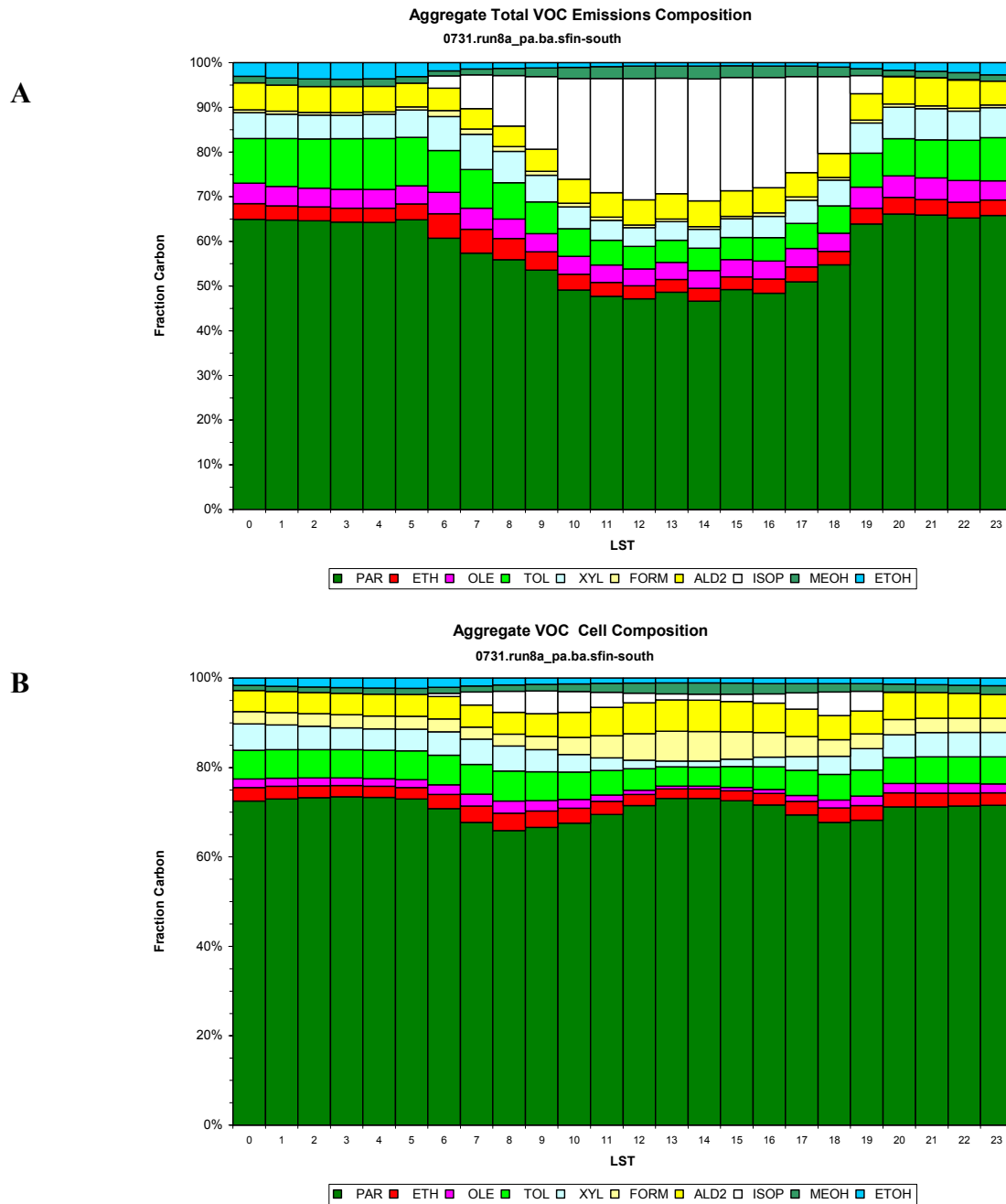


Figure 24. (A) Volatile organic compound percent composition of the process analysis box based on cell emissions, and (B) cell concentration as a function of time for the southern ozone region.

March 15, 2004

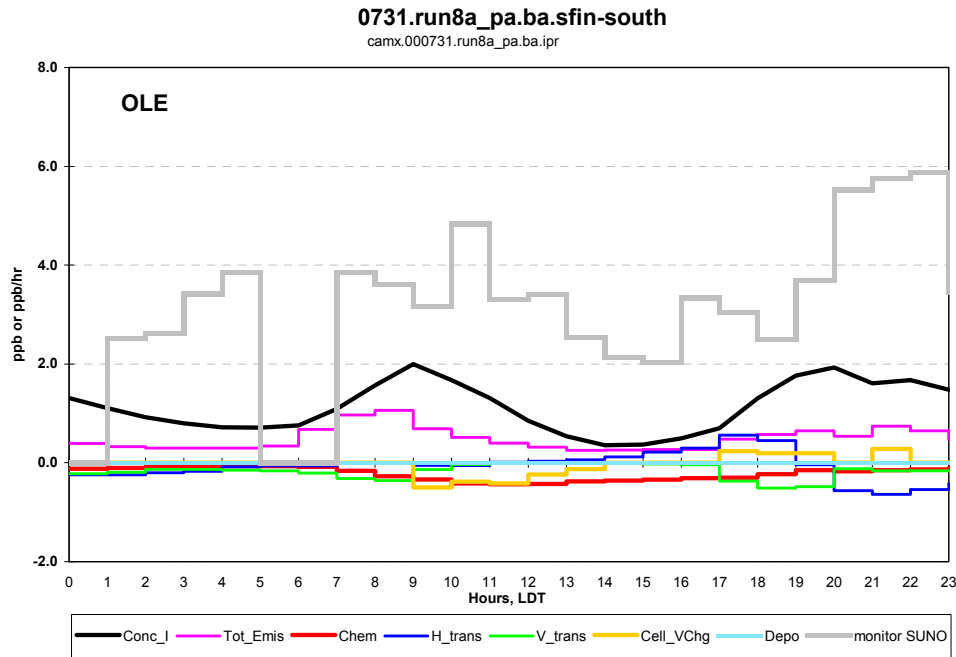


Figure 25. Olefin model concentrations and the processes that contribute to the final concentration for the southern ozone region. Observed data is shown from the Sunol (SUNO) monitor station as a one hour average.

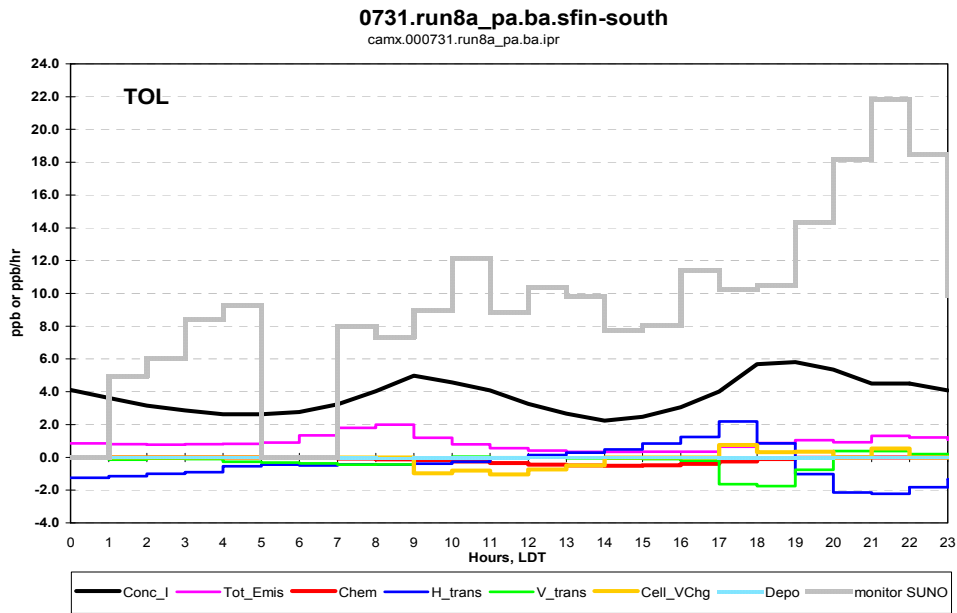


Figure 26. Toluene model concentrations and the processes that contribute to the final concentration for the southern ozone region. Observed data is shown from the Sunol (SUNO) monitor station as a one hour average.

March 15, 2004

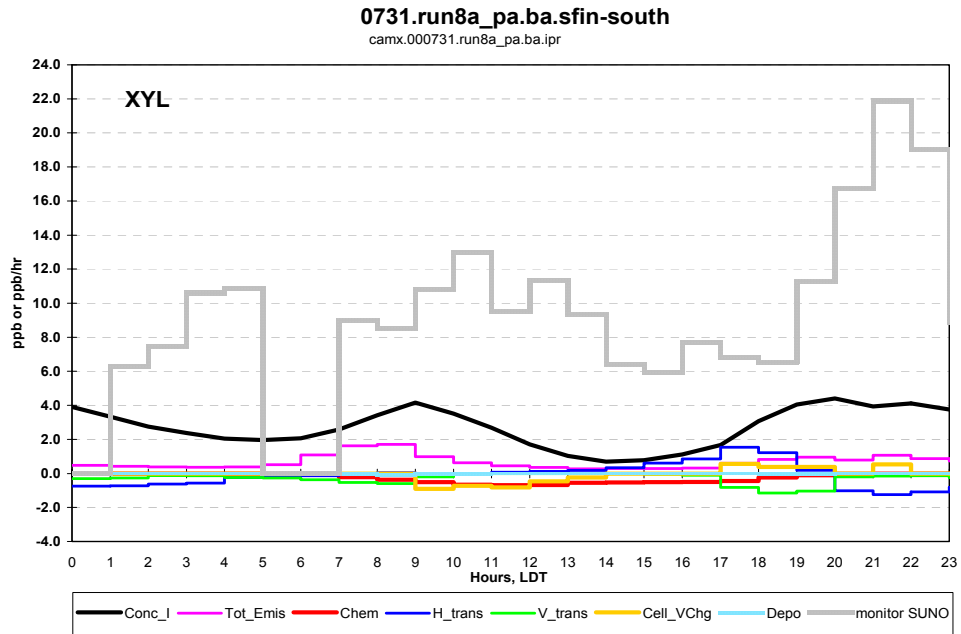


Figure 27. Xylene model concentrations and the processes that contribute to the final concentration for the southern ozone region. Observed data is shown from the Sunol (SUNO) monitor station as a one hour average.

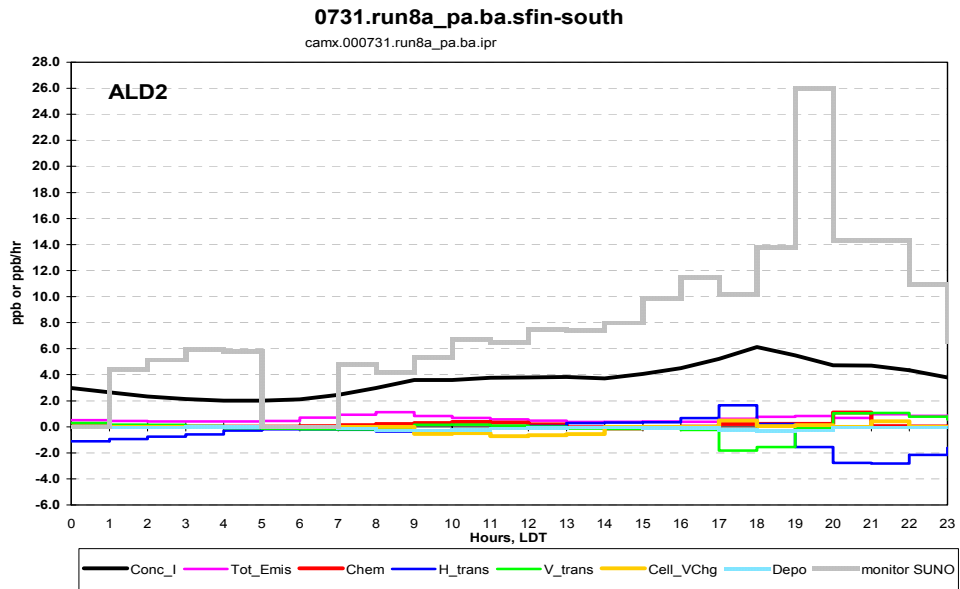


Figure 28. ALD2, a classification of aldehydes, model concentrations and the processes that contribute to the final concentration for the southern ozone region. Observed data is shown from the Sunol monitor station as a one hour average.

March 15, 2004

camx.000731.run8a_pa.ba.ipr
camx.000731.run8a_pa.ba.irr

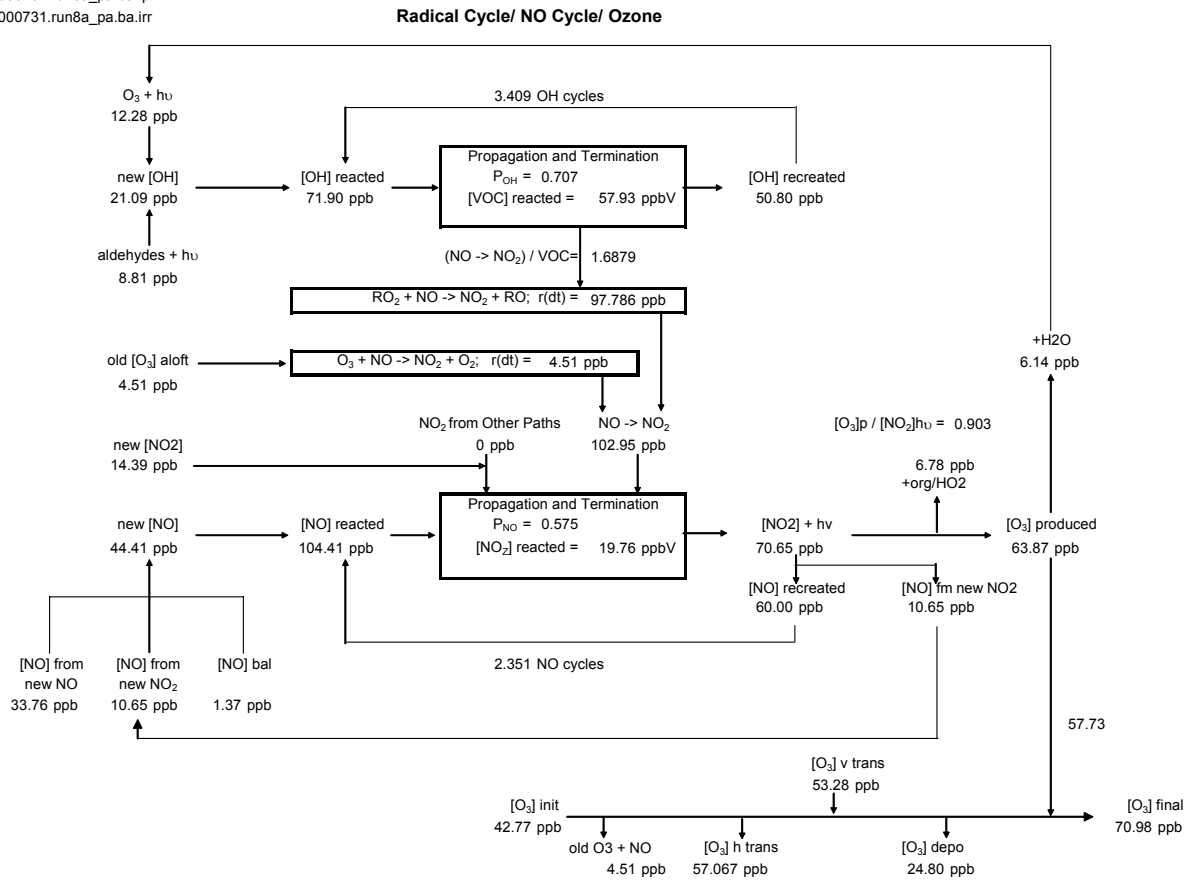
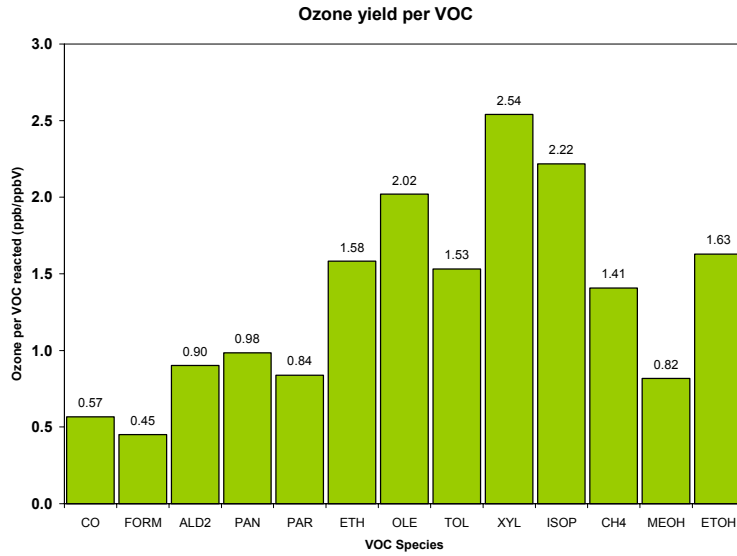


Figure 29. Ozone production diagram including radical and NOx cycles in the southern ozone region for hours 8-18.

March 15, 2004

A



B

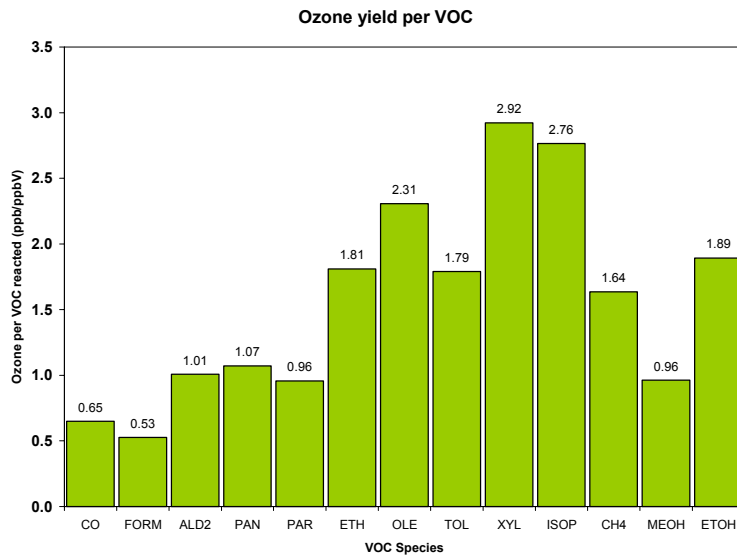


Figure 30. Ozone yield per VOC for hours 8-18 for (A) the northern source region and (B) southern ozone region.



March 15, 2004

camx.000731.run8a_pa.ba.ipr

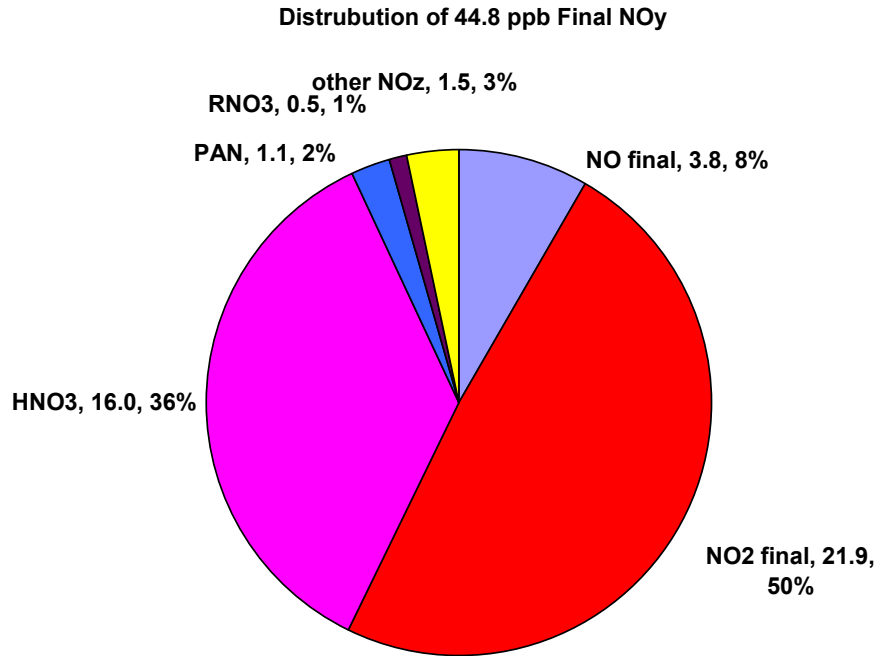


Figure 31. Distribution of the final NOy in the southern ozone region for hours 8-18.



March 15, 2004

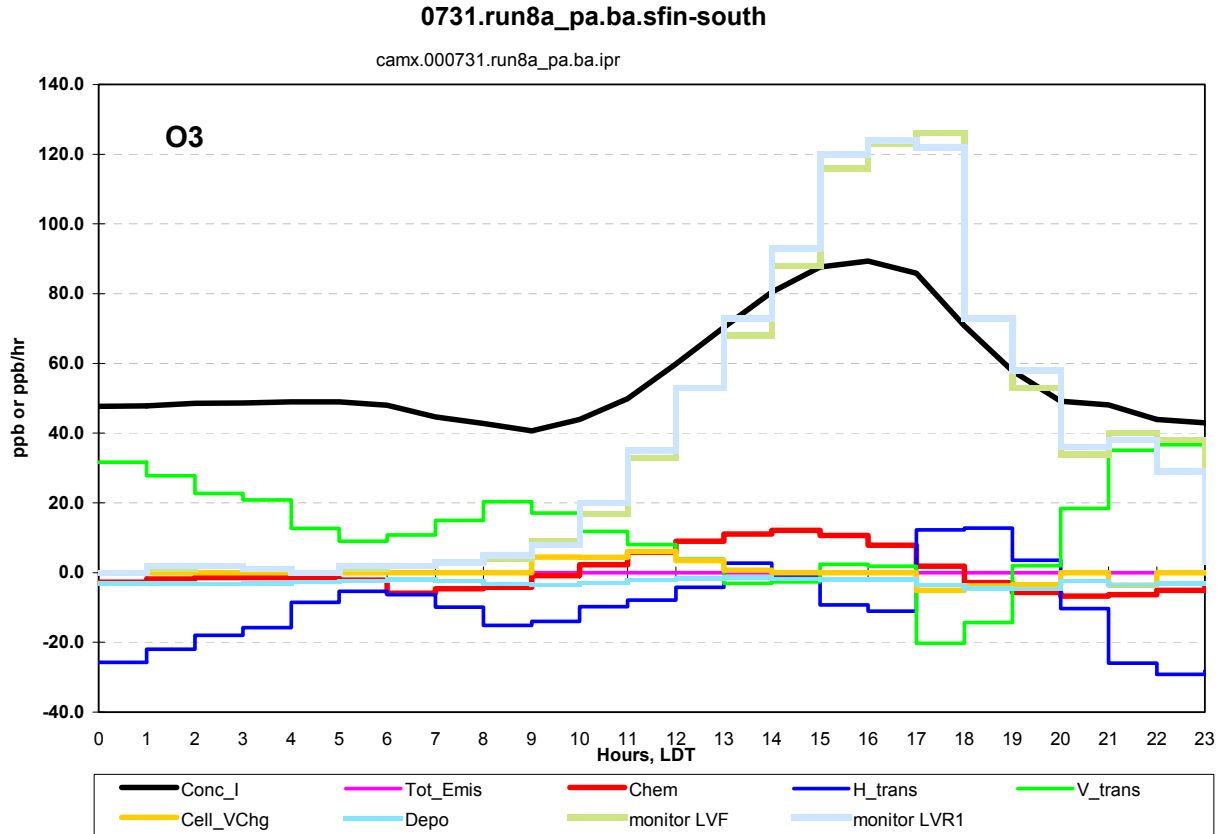


Figure 32. Ozone model concentrations and the processes that contribute to the final concentration for the southern ozone region. Observed data is shown from two Livermore monitor stations (LVF,LVR1) as one hour averages.